POLITECNICO DI TORINO

Corso di Laurea in Ingegneria Aerospaziale

Tesi di Laurea Magistrale

Mars Sample Return:

parking orbit optimization and single/multi launch mission comparison using genetic algorithm

Relatore
prof. Lorenzo Casalino

Studente
Gianmarco Floro
matricola: 254070

Aprile 2021

For my family

Abstract

This master thesis refers to the 'Mars Sample Return' space program currently underway by the collaboration of NASA and ESA. It is divided into three different missions: the launch of the rover 'Perseverance' for the collection of the samples, which landed this year on Martian soil, and the two missions currently under study, the first with the purpose of recovering the samples collected previously and inserting them into orbit (Sample Retrieval Lander - SRL), and the other one which will bring the samples back to our planet for analysis (Earth Return Orbiter - ERO).
The purpose of this master thesis is to select and analyse an orbit for a preliminary study of the SRL and ERO missions. Optimization of the orbit is performed by varying four parameters, namely the right ascension of the ascending node (RAAN), the longitude of the periapsis (LAN), and the position vectors of the capture and escape conditions. A genetic algorithm is then used, exploiting the 'Global Optimization Toolbox' of MATLAB, to minimize the initial mass, and, considering the initial conditions, to define the orientation of the orbit and the capture and escape positions related to the optimized case.
In the first part of the thesis, the background of the 'Mars Sample Return' campaign is presented, highlighting the reasons for the great interest in Mars, and defining the basis for the subsequent sections. The second part introduces the fundamental notions about genetic algorithms, including their application on MATLAB and terminology. In the next section is summarized the theory of the space flight mechanics necessary to understand the subsequent calculation procedures. Then, the problem is faced from a theoretical point of view, and the calculation methodology and the hypotheses considered during the work are detailed. In the last part of the thesis, the results of the work are presented, considering initially the hypothesis of performing both missions with a single launch, and then evaluating the two missions launched separately to estimate the advantages compared to the previous case.

Sommario

La presente tesi fa riferimento al programma spaziale ‘Mars Sample Return’ attualmente in corso da parte della collaborazione di NASA ed ESA. Esso è suddiviso in tre missioni differenti: il lancio del rover ’Perseverance’ per la raccolta del materiale, atterrato quest’anno sul suolo marziano, e le due missioni attualmente in fase di studio, ovvero quella che avrà lo scopo di recuperare i campioni raccolti in precedenza e inserirli in orbita (Sample Retrieval Lander - SRL), e la missione che riporterà i campioni fino al nostro pianeta per poterli analizzare (Earth Return Orbiter - ERO). Lo scopo di questa tesi è di selezionare e analizzare un’orbita marziana per uno studio preliminare delle missioni SRL ed ERO. L’ottimizzazione dell’orbita viene eseguita variando quattro parametri, ovvero l’ascensione retta del nodo ascendente (RAAN), l’argomento del periastro (LAN), e i vettori posizione delle condizioni di cattura e fuga. Viene quindi utilizzato un algoritmo genetico, sfruttando il ‘Global Optimization Toolbox’ di MATLAB, per minimizzare la massa iniziale, e, considerando le condizioni iniziali, si andrà a definire l’orientamento dell’orbita e le posizioni di cattura e fuga relative al caso ottimizzato.

Nella prima parte della tesi viene presentato il background della campagna ‘Mars Sample Return’, cercando di evidenziare i motivi del grande interesse verso Marte, e definendo le basi per le sezioni successive. Nella seconda parte vengono introdotte le nozioni fondamentali riguardo gli algoritmi genetici, compresa la loro applicazione su MATLAB e la terminologia. Nella sezione successiva viene riassunta la teoria della meccanica del volo spaziale necessaria per capire i procedimenti di calcolo successivi. In seguito, viene affrontato il problema dal punto di vista teorico e vengono dettagliate la metodologia di calcolo e le ipotesi considerate durante il lavoro svolto. Nell’ultima parte della tesi vengono esposti i risultati del lavoro, considerando inizialmente l’ipotesi di eseguire entrambe le missioni con un unico lancio, per poi valutare le due missioni lanciate separatamente per stimare i vantaggi rispetto al caso precedente.

Acknowledgements

Many thanks are owed to my thesis supervisor, Professor Lorenzo Casalino, for his guidance and assistance in the development of this work. A heartfelt thanks also to those who have been close to me on this long journey.

Contents

List of Tables

List of Figures

Chapter 1

Mars Sample Return Campaign

This Chapter describes the usefulness of the exploration of Mars and the objectives to be achieved in the next missions on the planet. The three missions of the 'Mars Sample Return' Program are briefly introduced as they are the example on which this thesis is based. The choice of the landing site chosen for these missions is also described.

1.1 Introduction

NASA's Mars Exploration Program (MEP) was announced by U.S. Space Agency (NASA) in 2000 with the purpose of exploring Mars through spacecrafts, landers and rovers [1]. The mission statement of the MEP is: *'The goal of the Mars Exploration Program is to explore Mars and to provide a continuous flow of scientific information and discovery through a carefully selected series of robotic orbiters, landers and mobile laboratories interconnected by a high-bandwidth Mars/Earth communications network'* [2].To support an integrated program structure, MEP carries out a number of activities that provide long-term investments for the future. One of the most ambitious goals of the MEP is the construction of a human outpost on Mars, however at the moment neither the technology nor the necessary knowledge are available. The attention of this thesis is in fact directed to a space campaign in full operation in this years, namely the 'Mars Sample Return' campaign. It has been decades since the exploration of Mars began and there have been truly remarkable technological advances since then regarding space probe instruments. However, it is not possible to obtain data as precise as those that would be obtained by studying the composition and characteristics of the Martian soil in the Earth laboratories. So, NASA and ESA signed a Joint Statement of Intent to carry out 'Mars Sample Return' Mission by means of an international partnership of returning Martian soil samples to Earth through a robotic mission.

1.2 Objectives

The Mars Exploration Program Analysis Group (MEPAG) has listed a document [3] in which are described the four main objectives to achieve with Mars exploration are:

- 1. *Determine if Mars ever supported, or still support Life*: the search for the presence of life on other celestial bodies is one of the most ambitious objectives of space exploration. Mars is certainly one of the best candidates because it has a relatively similar history to that of the Earth. The research carried out so far on the Red planet has discovered the presence of signs that identify the presence of water on the planet in the past. Future missions will therefore have to look for traces of the presence of water or residues of some chemical molecules that are traces of the presence of life, past or present, in Martian rocks.

- 2. *Understand the processes and history of Climate on Mars*: it is interesting to study the changes that the climate of Mars has undergone over time to reach the one present on the planet today. It is therefore important to understand what have been the processes that have characterized the Martian climate throughout its history. In fact, the climatic history of Mars has not always been like the current one, but in the 'recent' history of the planet (<20Mys) this planet had temperatures and pressures similar to those of Earth. In addition to this, the study of how the chemical composition of the atmosphere has evolved over time is a priority.

- 3. *Understand the origin and evolution of Mars as a Geological System*: as already mentioned, the history of Mars has traits similar to those of the Earth, for this reason it is essential to document the geological history of the Martian crust. In fact, it contains information regarding the phenomena that occurred during the history of the planet, such as volcanic activity. This goal is related to the previous objectives, because by studying the history of the crust, it is possible to find sediments that indicate the presence of water, or that there are records of activities related to climate changes. This could lead to an improvement in the information we also have in relation to our planet, of which many traces have been lost due to the high erosion activity.

- 4. *Prepare for Human Exploration*: one of the fundamental studies regarding Mars is preparing for future human missions. The risks are still many and are mainly due to the lack of knowledge. The risks were then classified according to the impact they have on costs and human safety and sub-objectives were drawn up. One of these is for example the study of how the Martian atmosphere impacts on the man landing. Another fundamental factor to be analyzed will be understanding how to organize and manage human extravehicular activities (EVA) and the exploitation of in-situ resources.

1.3 MSR Mission Architecture

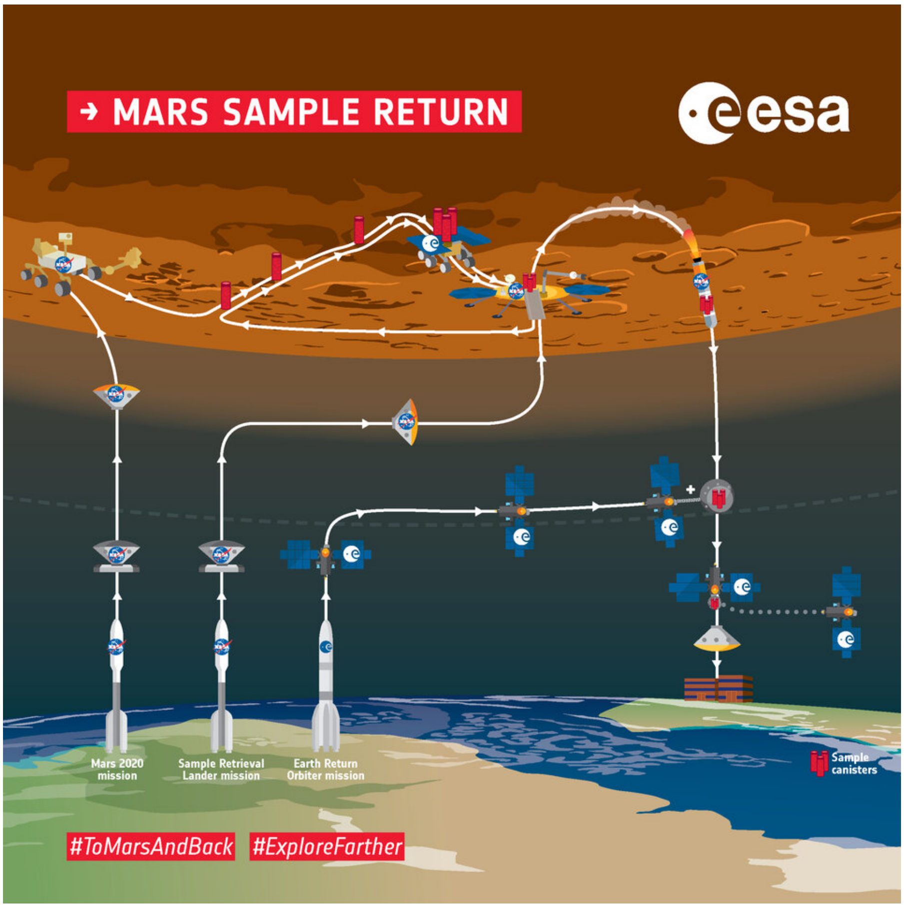

Figure 1.1: Mars Sample Return overview infographic. [5]

MSR architecture [4] [5] is composed by three different missions from 2021 to about 2031: the Mars 2020 catching samples rover, Perseverance has just landed on Mars; the second vehicle to arrive on the planet will be a Sample Retrieval Lander (SRL), whose rover will collect the samples left by Perseverance. SRL will have also a launch platform that will be use to launch the samples in Mars orbit. The last part of the mission is left to the Earth Return Orbiter (ERO), that will bring the samples back to the Earth [6]. An overview of the mission architecture of the entire mission can be seen in Figure 1.1. In the following paragraphs has been given a brief description of each of these missions.

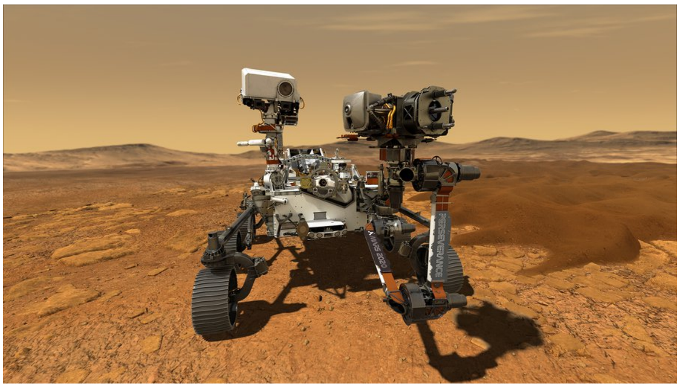

Figure 1.2: Illustration of NASA's Perseverance rover on Mars. Image Credit: NASA

1.3.1 Mars2020

The *Mars 2020* mission is the first of the MSR program. Its purpose is to collect samples from the Martian soil, thanks to the Perseverance rover, landed on Mars on 18 February 2021[7] [8]. Perseverance weights about 1050 kg and its configuration is based on that of its predecessor Curiosity, but its instrumentation is technologically more advanced. The purpose of the rover is to collect a minimum of 20 samples from the Martian soil thanks to its drill, and then seal them inside samples containers that will be deposited on the planet's soil. The samples will then be collected by the missions that will arrive later on Mars. A particularity of Perseverance is its robotic arm, over 2 meters long, which has five degrees of freedom and ends with a 'turret' containing cameras and instruments for analyzing samples. The rover also has instruments for technology demonstration. One of these is Ingenuity, a drone-helicopter that will perform the first flight on another planet to demonstrate flight stability even with a Mars rarefied atmosphere.

1.3.2 Sample Retrieval Lander

The *Sample Retrieval Lander* (SRL) is scheduled for 2026 launch [9]. It is composed by three different systems:

- the Sample Fetch Rover (SFR)
- the Mars Ascent Vehicle (MAV)
- the Orbiting Sample (OS)

The SFR will aim to collect the sample tubes left by Perseverance. the Rover has to be lightweight, from the preliminary studies it is estimated to be about 120 kg and, with a speed of about 200m/sol under nominal conditions, it will drive for

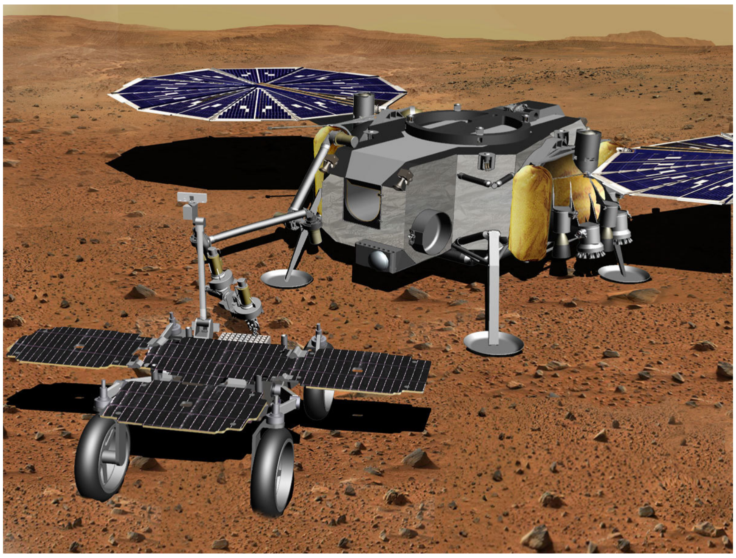

Figure 1.3: Illustration of the SRL components: in the foreground the SFR [2]

about 150 sol (Martian days). SFR would be completely autonomous in terms of navigation, and also be able to resists to the external environment, an example are sandstorms and cold conditions. After that phase, it will return to the SRL, where a Transfer Arm will deposit the collected samples into the OS, which will be next transfered to the MAV.
Mars Ascent Vehicle has to bring the OS to a circular Low Mars Orbit (LMO) with an altitude of about 400 Km [10], and will be the first vehicle to perform a launch on another planet. MAV is one of the key elements of the entire mission and there are two types of concepts regarding the type of propulsion to be used: hybrid propulsion or two-stage solid. The weight of the payload that will have to carry into orbit is about 16 kg and the challenge will be to minimize the weight at launch [4].
The Orbiting Sample has to contain the sample tubes and keep them safe from contamination. It will also have a thermal control system to keep the samples at the right storage conditions. As a further requirement, it must have a sufficiently high albedo value to be found by the ERO orbiter. This part of the mission will be the most challenging as the orbiter and the OS, must be in sight and have to be coordinate to complete the rendezvous maneuver.

1.3.3 Earth Return Orbiter

As for the *Earth Return Orbiter* (ERO), it will have the purpose of communicating with the other components of the mission present on Mars; moreover, it will have to be able to independently manage the recovery of the OS in orbit before returning

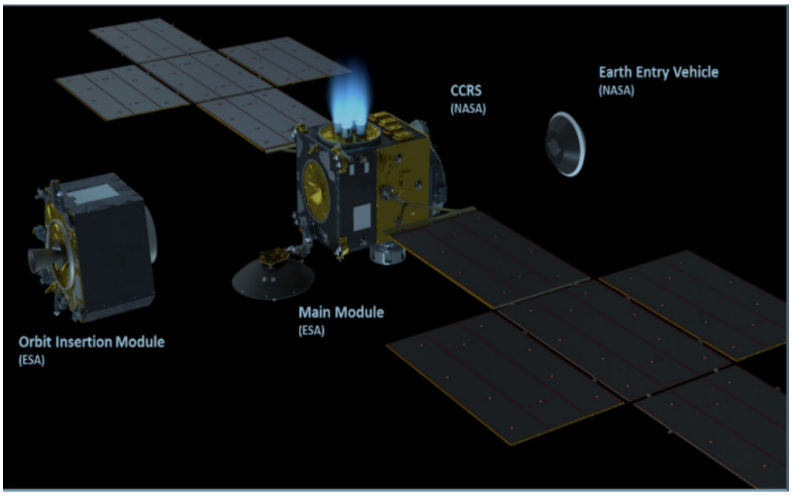

Figure 1.4: Illustration of the ERO Main Systems [4]

to Earth [4] [6].
ERO will be developed by ESA and will use chemical propulsion for the outward phase to Mars and electric propulsion for the return. One of its most important part is the Containment/Contamination and Return System (CCRS). It in turn includes three distinct parts:

- the Capture Orient Module (COM), which would capture the OS e transfer it to the Containment Module;
- the Containment Module (CM), that would secure the sample tubes from any type of contamination;
- the Earth Entry System (EES), that receives the tubes thanks to a robotic arm installed on the main module, and places them safe for the return maneuver. EES is being designed with the capability to land on the Earth without parachute, but only with passive aerodynamics [4].

The chemical thruster used for the transfer to Mars, the Orbit Inserction Module, is separated when the final destination is reached. At the beginning of escape from the planet, for reason of mass saving, the CM and COM are jettisoned, so the only vehicle to return to Earth is the EEV.

1.4 Landing Site

Between 2014 and 2018, scientists discussed about which Martian site was best suited for collecting samples, comparing more than 30 different Mars locations, and finally the decision felt on *Jezero Crater* (in Figure 1.5). Jezero area is an

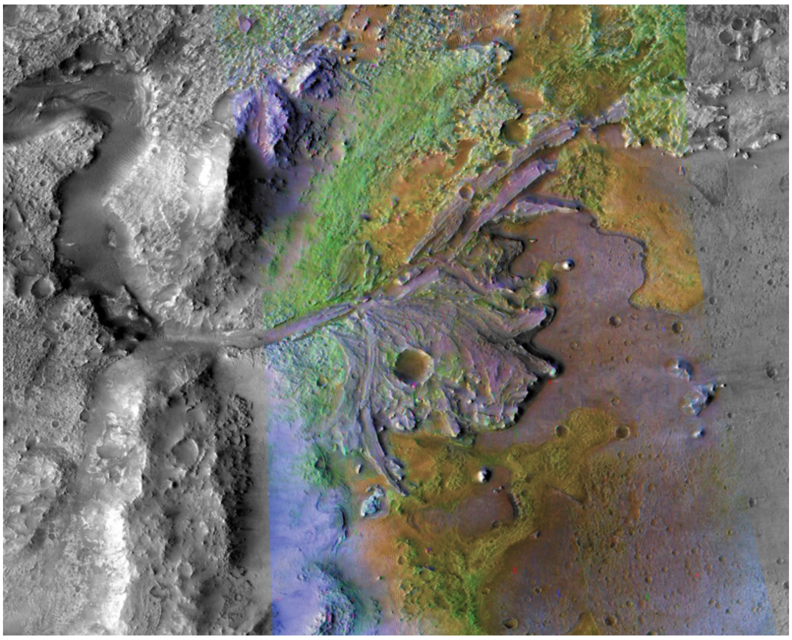

Figure 1.5: Image of Jezero Crater taken by MRO (Mars Reconnaisance Orbiter). Image Credit: NASA

impact crater of 45 Km in diameter, located at approximately 18° Nord, 77° East, in a region of Mars known as Nili Fossae and has been selected because it contains elements thought to have been shaped by liquid water in the ancient past of Mars [11]. The area near the crater, in fact, has some very interesting features, such as well-preserved river delta deposits, inlet valleys and also an outer channel. In a period called *Noachian Age* probably this was a lake.
Mars Reconnaissance Orbiter MRO was a spacecraft launched in 2005, and it made observations that helped scientists to understand the history of liquid water on Mars. The instrument on board of MRO is the CRISM, and was designed to identify minerals on Mars that formed in the presence of water thanks to the observation of light reflected from the Martian surface. Many Mars missions have provided evidence that liquid water once flowed on the surface of the red planet, but MRO data can contribute to help the understanding of how long this water persisted.

Chapter 2

Genetic Algorithm

Evolutionary Algorithms (EA) are a type of artificial intelligence; they consists of a population of potential solutions which evolves to a better solution generation after generation. These algorithms were developed for Evolutionary Computing, inspired by Darwin's Evolution Theory, that through the use of natural selection, adaptation and survival laws find the best solution.[12][13]
Genetic Algorithms (GA) are the most popular type of EA and are widely used to solve optimization problems. They were developed for the first time by Nils Barricelli in 1953 [14], with the purpose to create artificial life inside a computer by using processes found in nature. Individuals more suitable than a given population are those who are likely to have a chance to survive and reproduce, thus transmitting its characteristics to the offspring. Consequently, subsequent generations will exhibit a degree of greater fit and will be better. This process can be applied to a problem starting from a random population and progressively combining the best individuals to each generation, generating progressively better new populations. This mechanism allows to find useful solutions without the evaluation of all the different combinations offered by the research space. This proves to be particularly useful when the number of possible solutions is very large, as in the case of this master thesis. An algorithm with a strong evolutionary component tends to be faster and to reach convergence first but may have trouble finding the global minimum and rather converge to a local minimum. Instead, giving a strongly random imprint to the code search process, you manage to have a better exploration of the space of solutions but sacrificing speed of the code itself.

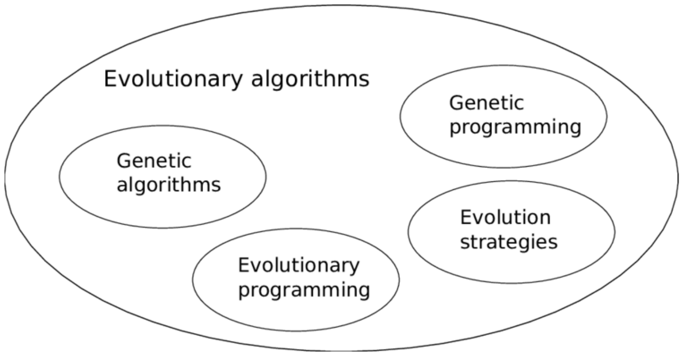

Figure 2.1: Classification of Evolutionary Algorithms

2.1 Terminology

In order to better describe the process by which these algorithm works, the basic terminology , which derive directly from biologics and genetics, is reported below:

- Population: it is the set of individuals involved in the search process.
- Individual: is a single solution to the problem that the genetic algorithm is trying to solve. It is composed by the genotype which contains the genetic information, and the phenotype that is the expression of the individual in terms of the model.
- Gene: it is one of the elements of an individual.
- Feature or allele: it is the value a gene takes for a particular chromosome
- Genetic operators: they alter genetic composition of the offspring.
- Fitness function: for standard optimization algorithms, this is known as the objective function. It gives a fitness score to each individual. The probability that an individual will be selected for reproduction is based on its fitness score.
- Son: it is the results of the reproduction process that belongs to the next population as a member.
- Decoding - Encoding: Decoding is a process of transforming a solution from the genotype to the phenotype space, while encoding is a process of transforming from the phenotype to genotype space.

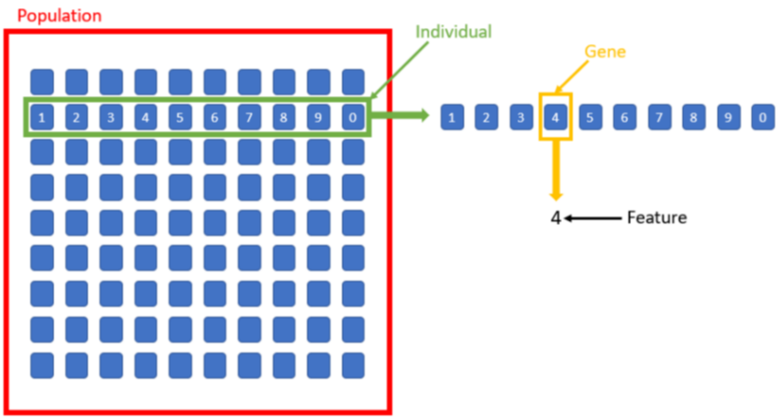

Figure 2.2: Genetic algorithm terminology scheme

2.2 Operating Method

The general structure of a genetic algorithm process is rapresented in Fig.2.3 and could be summarized as follow:

- Encoding
- Evaluation
- Crossover
- Mutation
- Decoding

The crossover phase involves the construction of the iteration population starting from the elements with the highest degree of fitness. Here the methodologies are many and will be discussed in detail in the following sections. Finally there is the phase of mutation; in fact it is always necessary to guarantee a certain variability within a population to avoid phenomena of premature convergence or cases in which the algorithm remains trapped in its surroundings of a local minimum.
Once the entire process is completed, the previous population is replaced with the next one and start all over again. In addition it is necessary determine when to stop the genetic algorithm.

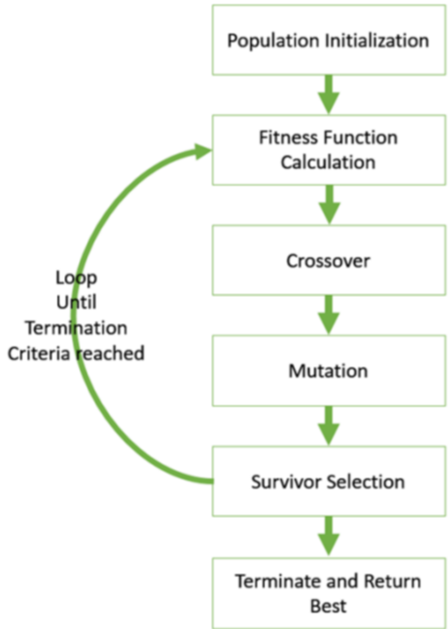

Figure 2.3: Genetic algorithm process [15]

2.3 Initial Population

The first step in the functioning of a genetic algorithm is, then,the generation of an initial population. Population sizing is one of the most important topics to consider in evolutionary computation. In fact, a small population size could guide the algorithm to poor solutions and a large population size could increase algorithm computation time.

2.4 Fitness Function

In most cases the fitness function and the objective function are the same as the objective is to either maximize or minimize the given objective function. However, for more complex problems, the designer might choose to have a different fitness function. A fitness function should be sufficiently fast to compute and it must quantitatively measure how fit a given solution is or how fit individuals can be produced from the given solution. In some cases, is not possible to calculate the fitness function directly due to the complexities of the problem, so fitness approximation is made to suit the needs. Calculation of fitness value is done repeatedly, and therefore it should be sufficiently fast. A slow computation of the fitness value can adversely affect the algorithm and make it exceptionally slow.

2.5 Parent Selection

Parent Selection is the process of selecting parents which mate and recombine to create off-springs for the next generation. Parent selection is very crucial to the convergence rate of the GA as good parents drive individuals to a better and fitter solutions.

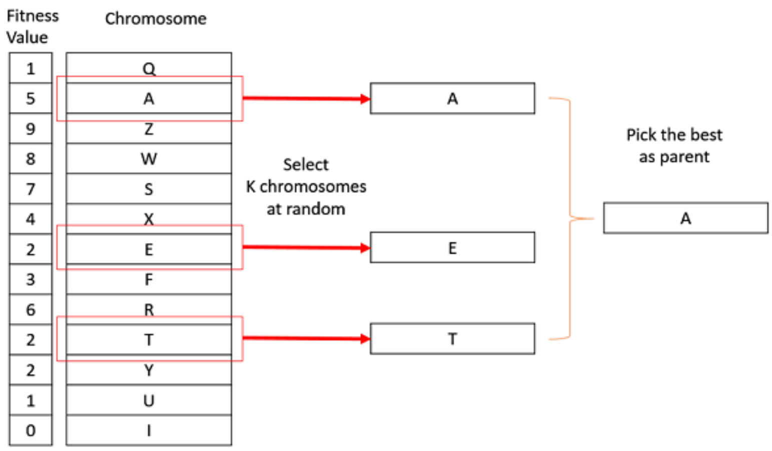

Figure 2.4: Tournament Selection [15]

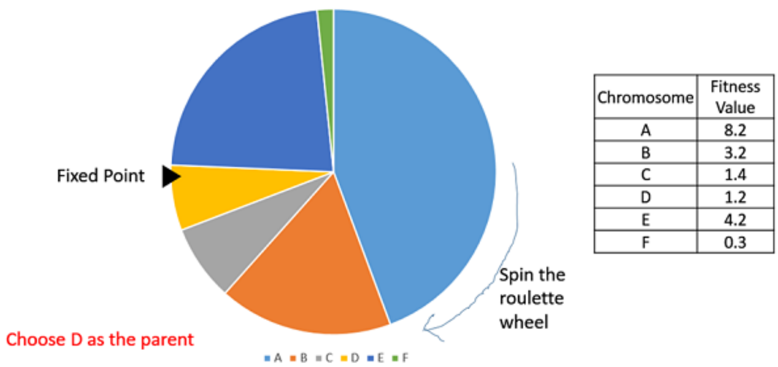

Figure 2.5: Roulette Wheel Selection [15]

Tournament Process

This type of selection is one of the most popular because it is very simple to implement but also quite efficient. In the tournament selection there are 'n' elements chosen randomly from the population and then they are subsequently made compete against each other; the winning chromosome is chosen for the crossover. The number of challengers can vary but usually it is used a binary type tournament with only two participants. In this way, the selection process allows to maintain the diversity between the elements selected and each chromosome is chosen without benefiting the best. Other advantages are the speed from the computational point of view, a low probability that dominant elements could monopolize the group of selected and finally no need for sorting the fitness or to have to normalize it in some way.

Proportional roulette wheel selection

In the proportional roulette selection, individuals are chosen with a probability that is directly proportional to one's fitness value and therefore it is possible to think of a roulette where the number of times that each chromosome appears is linked to how high its fitness value is. This obviously implies that items with a higher fitness level occupy larger portions of roulette. When the wheel is spun, it will tend to stop with good probability with the pointer directed towards one of the individuals with higher fitness value. The process must be repeated as many times as desired use for crossover. The main advantage of proportional selection is related to the fact of not discarding any element of the population and therefore giving everyone the possibility of being selected. There are also some important disadvantages: for example, the presence of a very high fitness elements compared to the others can cause a premature convergence of the code.

Best Only Selection

Unlike previous methods which rely on probabilistic mechanisms, this type of selection is the most drastic. The final population contains only the best chromosome repeated as many times as the user's preference. In this case, individuals are not subjected to crossover, but they are directly promoted to mutation stage. This choice leads genetic algorithm to exasperate its functioning by turning it into a local randomized research.

2.6 Reproduction Process

2.6.1 Crossover

The crossover is the mechanism by which individuals are created for the next iteration starting from the winners of the selection process. The term 'parent' is used for the input chromosomes and 'children' for the output chromosomes. The crossover, to be effective, must allow the transfer of promising genetic material and perform a scrambling to obtain even better solutions in the future. There are many methods for this process and, since the code used is combinatorial, the main techniques are proposed in the next subsection.

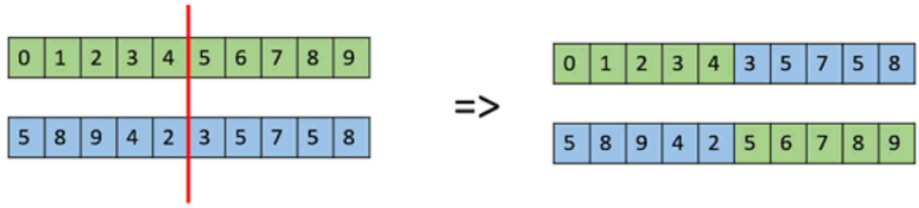

(a) *Single Point*

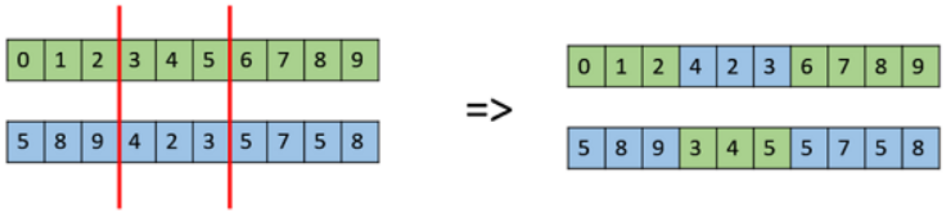

(b) *Multi Point*

Figure 2.6: Examples of Crossover Techniques [15]

Single Point Crossover

This is the simplest possible technique; it begins by randomly selecting an element (or gene) of a parent and positioning it in a random new position, in the child. Then, the remaining elements of the parent are inserted in the same order in which they appeared before. An example is reported in Figure 2.6a. Multi-Point Crossover is also possible, and it is a generalization of the Single-Point.

City Centered Crossover

This type of crossover is based not so much on the choice of a random index, as on the choice of a debris. Thanks to this choice, the children inherit the same sequence of debris preceding the one selected. First, a gene is chosen, and it is searched for within the parents; at this point the genes are copied up to the selected one. Finally, the process is completed by completing the permutation through cross-filling (genes of the father in the daughter and genes of the mother in the son) always trying to keep the order unchanged.

Ordered Crossover

Sometimes it can be useful to try to pass on a certain potentially valid block of information to subsequent generations; you can therefore use this strategy; two indices are randomly chosen, and the elements included between the two indices in the child chromosomes are copied. At this point the chromosomes are completed again with a cross-filling trying to keep the order unchanged.

Order Based Crossover

The operation of this technique is based on the transfer of sub-sequences of genes that may contain good information. First, a certain number of indices are chosen in the mother and the corresponding vertices of the father are marked. The elements of the father that have not been deleted are then copied into the child and finally the marked elements of the mother are also reported, possibly in the same order.

2.6.2 Mutation

As already mentioned in the introduction, the mutation operator allows to maintain a certain degree of diversity within the population. Although the crossover functions correctly and guarantees a high degree of mixing, it cannot prevent a progressive homogenization of the vectors. In the advanced stages it is in fact probable that a small group of individuals possess very high fitness values and dominate in the selection stage. The mutation is therefore responsible for inserting completely new elements at each iteration whose genes can, once recombined, lead to the construction of even better individuals. Again, multiple strategies are available.

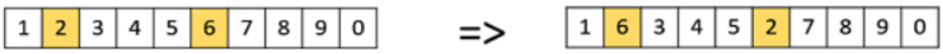

(a) *Single Swap*

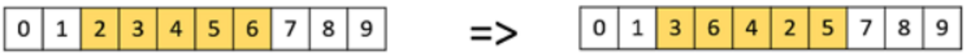

(b) *Scramble*

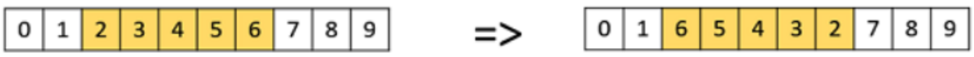

(c) *Swap Blocks*

Figure 2.7: Examples of Mutation Techniques [15]

Single Swap

This type of mutation simply selects two indices of the incoming chromosome (stochastically) and swaps the genes indicated by them. An example is shown

in Figure 2.7
In another case, the mutation chooses two indices of the input vector. The first number indicates the position of the information to be moved while the second indicates the position to which it must be moved. Finally, all that remains is to scale the elements between the two indices.

Scramble

Two indices are chosen at random and the elements between the two indicated extremes are randomly permuted. An example is reported in Figure 2.7b, in which the chosen values are 2 and 6.

Swap Blocks

Two indices have been chosen to determine a division of the chromosome into three different sections. The first and third are therefore reversed while keeping the second unchanged. A mutation of this kind tends to keep any groupings of genes with good fitness characteristics intact, which could then help the code to build better elements in the next iteration.

2.7 Stopping Criteria

The termination condition of a Genetic Algorithm is important in determining when a GA iterations will stop. The algorithm progresses very fast with better solutions in every few iterations, but this tends to saturate in the later stages, where the improvements are very small. For this reason, it is implemented a stopping condition such that the solution is close to the optimal, at the end of the run. Below are listed the existing stopping criteria; GA stops:

- when there has been no improvement in the population for X iterations.
- when reaches an absolute number of generations.
- when the objective function value has reached a certain pre-defined value.

Like other parameters of a GA, the termination condition is highly problem specific, and the user should try out various options to see what suits his particular problem the best.

2.8 Genetic Algorithm in MATLAB

MATLAB is a programming platform that can be used for various purposes, including matrix computing, algorithm creation, simulation, and analysis. In the case of this master thesis, the interest is towards one of the MATLAB toolboxes: the *Global Optimization Toolbox*. "Global Optimization Toolbox provides functions that search for global solutions to problems that contain multiple maxima or minima"[16]. In particular, has been used the *ga* solver, which exploits the genetic algorithm principles. *ga* finds the minimum of a given function and it can be called in MATLAB with the following syntax:

```
[x, fval, exitflag, output, population, scores] =
ga(fun, nvars, A, b, Aeq, beq, lb, ub, nonlcon, options)
```

This parameters can be described as follows [16]:

- x : is the best point that ga localizes in its iterations, so is the local unconstrained minimum;
- $fval$: is the fitness function value calculated in x;
- $exitflag$: is an integer number that identifies why *ga* stopped;
- *output*: contains information about the optimization process;
- *population*: return a matrix containing the final population, where the rows are the individuals;
- $scores$: is a vector containing the final scores of the rows of population;
- fun: is the objective function;
- $nvars$: the number of variables;
- A: is the linear inequality matrix $A * x <= b$, where x is the column vector of the variables;
- b:is the linear inequality vector;
- Aeq: is the linear equality matrix $Aeq{*}x <= beq$, where x is the column vector of the variables;
- beq:is the linear equality vector;
- lb: is a vector that contains the lower bounds that the variables can assume;
- ub: is a vector that contains the upper bounds that the variables can assume;

- *nonlcon*: is a function containing nonlinear constraints;
- *options*: contains the optimization options defined by the user. If not specified, *ga* uses the default options.

With *optimoptions* MATLAB function the user can specify population dimensions, running time and many other options of genetic algorithm. Those used for the study carried out in this thesis are reported below:

- *SelectionFcn*: it is possible to specify a built-in function or a function handle that selects parents of crossover and mutation children;
- *EliteCount*:identifies the number of best individuals who will pass on to the next generation;
- *CrossoverFraction*: specifies the portion of the population created with crossover in the next generation, excluding Elite individuals;
- *PlotFcn*: it is possible to specify which built-in function will be used for plot algorithm data;
- *InitialPopulationRange*: specifies the range of initial values for initial data. It can be a vector or a matrix;
- *MigrationDirection*: can control how the migration between subpopulations occurs; it is possible to set a *ForwardDirection* if the subpopulation goes from the current to the next. The other possibility is the *Both* directions, in which subpopulation can move in the next or the previous one.

Chapter 3

Space Flight Mechanics

This chapter focuses on illustrating the fundamental concepts of space flight mechanics to help understand the work of this thesis.
In particular, have been invoked the concepts relating to reference systems, the equation of the trajectory, the conic sections and the orbital parameters. In the final part, the main phases of interplanetary maneuvers are presented.

3.1 Trajectory Equation

In order to introduce the law that regulates the motion of a body in orbit it is necessary to make a brief digression to mention the so-called "*two-body problem*". The assumptions made for this model are as follows:

1. Mass of the orbiting body m is negligible in respect of the attratting mass M;
2. The bodies are spherically symmetric, so that their masses can be considered as concentrated at their centers;
3. Only the gravitational forces between the two bodies are considered.

Using an inertial reference system, the relationship that describes the relative motion between the two bodies can be written as:

$$\ddot{\mathbf{r}} + \frac{\mu}{r^3}\vec{r} = 0 \tag{3.1}$$

where r is the distance between the two bodies, and μ is defined as (3.2) and it is the *gravitational parameter*, different for each planet. For Mars the value of μ is 42828 Km^3/s^2.

$$\mu = GM \tag{3.2}$$

The gravitational field is conservative and this means that there is a conservation of mechanical energy. The energy that a certain mass possesses in a gravitational field, without the influence of external forces, is given by a balance of kinetic energy and potential energy. The expression of the specific mechanical energy is:

$$\epsilon = \frac{V^2}{2} - \frac{\mu}{r} \tag{3.3}$$

The first term of the (3.3) refers to the kinetic energy per unit of mass and the second to the gravitational potential energy per unit of mass. For this reason ϵ is a so-called "*constant of motion*". Another quantity that remains constant during the motion is the specific angular momentum $\vec{h}$.

$$\vec{h} = \vec{r} \times \vec{v} \tag{3.4}$$

Since $\vec{h}$ is the vector product of two quantities, it will always be perpendicular to the plane containing $\vec{r}$ and $\vec{v}$. Since $\vec{h}$ is constant, these $\vec{r}$ and $\vec{v}$ will always lay in the plane of motion, that is defined *orbital plane*. The specific angular momentum vector is also expressed through the relation in (3.5), in which the angle between the direction of the velocity and the plane of the horizon appears. This angle is called the *flight-path angle*. The complementary angle of γ is called the *zenith angle* ϕ, defined as the angle that the velocity forms with the local vertical

$$\vec{h} = rv \sin\gamma \tag{3.5}$$

$$\vec{h} = rv\cos\phi \tag{3.6}$$

Thanks to these considerations it is now possible to integrate the equation in (3.1)

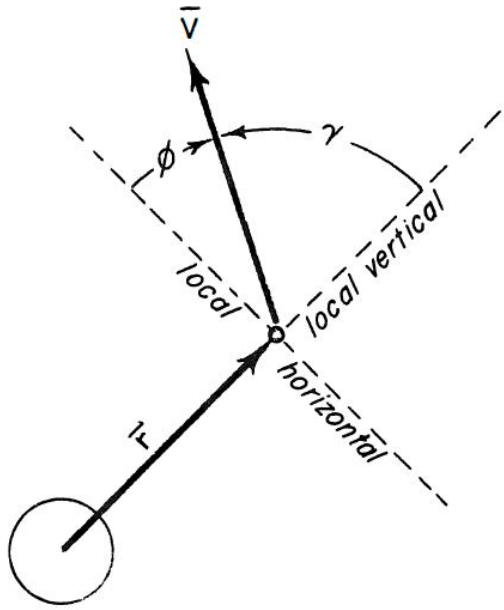

Figure 3.1: Flight-path Angle and Zenith Angle [17]

to obtain the trajectory equation, which expression is:

$$r = \frac{\frac{h^2}{\mu}}{1 + \frac{B}{\mu}\cos\nu} \tag{3.7}$$

- h is the magnitude of specific angolar momentum;
- μ is the gravitational parameter;
- B is the constant of integration vector. It points towards the direction of minimum distance between the trajectory and the main focus. This distance is called *periapsis*;
- ν is the *true anomaly*, the angle between the direction of the periapsis and position vector $\vec{r}$.

3.2 Conic Sections

The expression in (3.7) contains information about the dynamics and kinematics of the satellite motion. It is possible to write a similar equation which contains

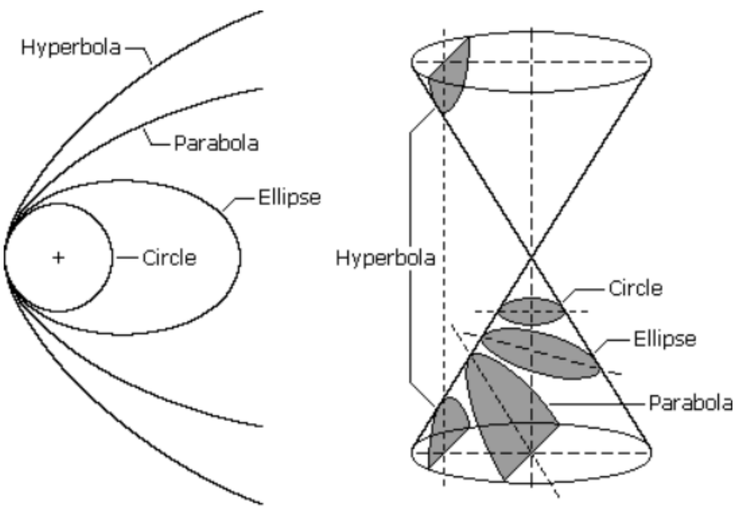

Figure 3.2: Types of Conics Sections and Related Orbital Trajectories

information relating to the geometry of the trajectory. This equation can be seen in (3.8).

$$r = \frac{p}{1 + e \cos \nu} \tag{3.8}$$

in which:

- p is the *semilatus rectum*, a geometrical constant of conic sections;
- e is the eccentricity.

There is a relationship between the expressions (3.7) and (3.8) and it is therefore possible to relate the kinematic and geometric quantities.

$$p = \frac{h^2}{\mu} \qquad e = \frac{B}{\mu} \tag{3.9}$$

The concept of conic section is now introduced as the locus of points such that the ratio of the distance from a fixed point called *focus* and a fixed line, said *directrix*, is constant and equal to e. Thus, from the value of the eccentricity it is possible to establish the type of conic. If the eccentricity is $e > 1$ then is considered an hyperbolic trajectory, while if it is exactly $e = 1$ the conic is a parabola, and if it is $e < 1$ an ellipse; eccentricity value equal to 0 refers to the circular orbit, which is a particular type of ellipse.
Another way to describe conic sections is as curves obtained from the intersection

of a cone and a plane. As can be seen from Figure 3.2[1], the different categories of conics are generated cutting the cone at different angles.
There are some geometric properties that are in common between the various families of conics. For example, all these curves have two foci, even if in the parabola the second focus is placed at an infinite distance from the first. In orbital mechanics, the most massive body, around which the trajectory takes place, is in one of the two foci, while the other has no physical meaning.
One of the main parameters of these curves is the semi-major axis a, which is the half length of the chord passing through the two foci. Another reference length is the distance between the two foci c, from which derives the expression that defines the eccentricity

$$e = \frac{c}{a} \tag{3.10}$$

We can therefore locate the two extremes of the semi-major axis, which are defined as *apses*. The distance of the closest point from the first focus is called *periapsis* and indicated by r_p, the expression of which is

$$r_p = a(1 - e) \tag{3.11}$$

Instead, the *apoapsis* r_a is the furthest point from the focus.

$$r_a = a(1 + e) \tag{3.12}$$

In the previous section has been said that the total specific mechanical energy is constant during the motion, and for all conic orbits is always valid that

$$\epsilon = \frac{v^2}{2} - \frac{\mu}{r} = -\frac{\mu}{2a} \tag{3.13}$$

The equation shows that the semi-major axis a depends only on the specific mechanical energy. This implies that ϵ has to be negative for closed orbits (circular or elliptic), while is equal or greater than zero if the orbit is parabolic or hyperbolic. Therefore,it is possible to summarize these concepts in a table:
The elliptic and hyperbolic orbits are presented, while the parabolic ones are excluded, because they are beyond the scope of this thesis.

3.2.1 Elliptical Orbit

Ellipse represents the typical trajectory that planets have in their revolution motion around the Sun. It is a closed orbit, so a body moving on an ellipse will always

[1]Image from http://www.braeunig.us/space/orbmech.htm

Conic Section	e	a	ϵ
Ellipse	$0 < e < 1$	>0	<0
Circle	0	>0	<0
Parabola	1	∞	=0
Hyperbola	>1	<0	>0

Table 3.1: Characteristic Parameters of Conic Sections

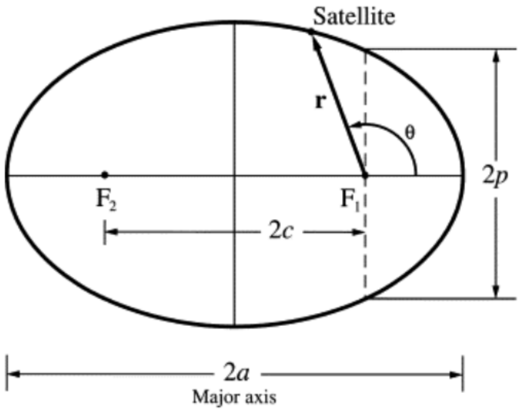

Figure 3.3: Elliptical Trajectory [18]

follow the same path. The time it takes for a body to complete the entire turn of an ellipse is called *orbital period* τ. Semi-major axis and eccentricity can be expressed through the periapsis and apoapsis distances with the following expressions:

$$a = \frac{r_p + r_a}{2} \tag{3.14}$$

$$e = \frac{r_a - r_p}{r_a + r_p} \tag{3.15}$$

The orbital period, instead, is a function of the geometry of the ellipse, in particular of the length of the semi-major axis. It can be written that:

$$\tau = 2\pi\sqrt{\frac{a^3}{\mu}} \tag{3.16}$$

3.2.2 Hyperbolic Orbit

This conic represents the trajectories commonly used for the capture, escape or fly-by maneuvers of a spacecraft.
The hyperbola has two branches, but only one of the two represents the one that

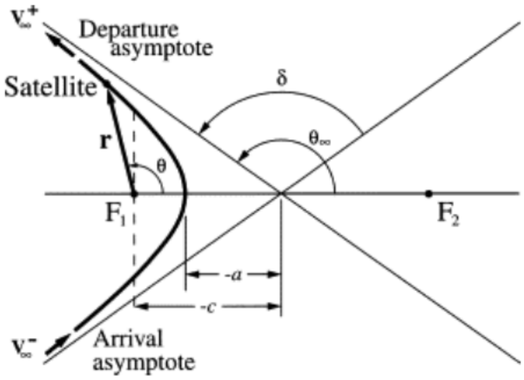

Figure 3.4: Hyperbolic Trajectory [18]

can actually be traveled. Referring to Figure 3.4, it is possible to indicate δ as the angle between the two asymptotes. This angle is related to the geometry of the hyperbola and therefore to the eccentricity, with which it has an inverse proportionality relationship.

$$sin(\frac{\delta}{2}) = \frac{a}{c} = \frac{1}{e} \tag{3.17}$$

Another important parameter is the hyperbolic excess speed V_∞. The minimum velocity needed to perform an escape from a planet is called *escape velocity* V_{esc}. If the spacecraft has this velocity, then it will exit the gravitational field of the planet with zero velocity and will perform a parabolic trajectory. Consequently, to go to a hyperbolic orbit will be necessary to have a speed greater than the escape velocity.

$$V_\infty^2 = V_{burnout}^2 - V_{esc}^2 \tag{3.18}$$

where $V_{burnout}$ is the speed of the spacecraft at the beginning of the maneuver.

3.3 Coordinates Systems

A coordinate system is always defined by an origin, a *fundamental plane* (X-Y) and the direction of two main axes, usually X and Z.
There are various types of reference systems for locating an object in orbit. The most suitable system will be chosen based on the problem. The following are those used in the context of this thesis and are described in the next subsections.

3.3.1 Perifocal Coordinate System

It is the most used coordinate frame for describing the motion of a satellite [17]. This is unique for every orbit and his foundamental plane is the orbital plane itself.

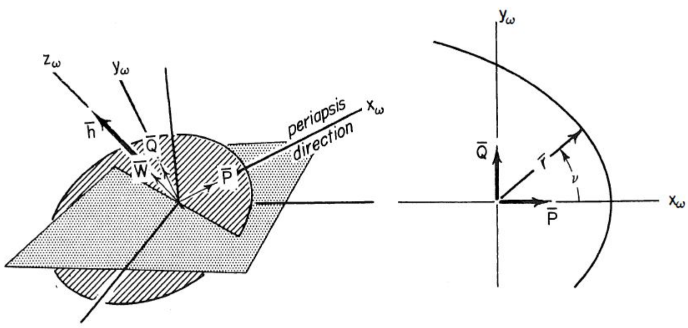

Figure 3.5: Perifocal Reference System [17]

The origin is located in tha main focus of the conic section, usually the center of a planet.
The X-axis is directed towards the pariapsis, the-Z axis lies in the direction of the vector $\vec{h}$ and Y-axis lies on the plane of the orbit and is inclined 90° in the direction of the motion. Unit vectors in the X, Y and Z direction are called respectively P, Q and W.

3.3.2 Equatorial Coordinate System

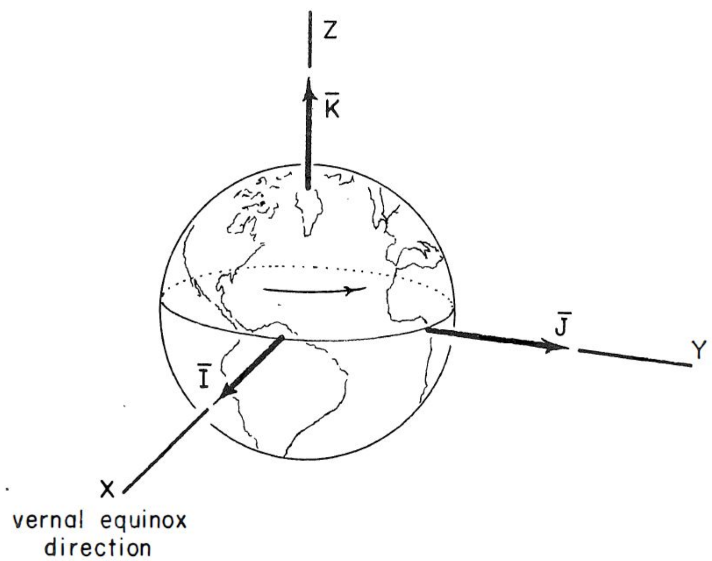

Figure 3.6: Equatorial Reference System [17]

It is also known as 'Geocentric-Equatorial' as applied on Earth. It has its origin in the center of planet, in this case Mars, and its foundamental plane is the equator, in which lays X and Y. Unit vectors in direction X,Y and Z are named I,J,K. The X-axis points in the vernal equinox direction, thus towards the Aries constellation. Z-axis is directed to the North Pole direction and Y-axis completes the triad.

3.3.3 Right Ascension-Declination Coordinate System

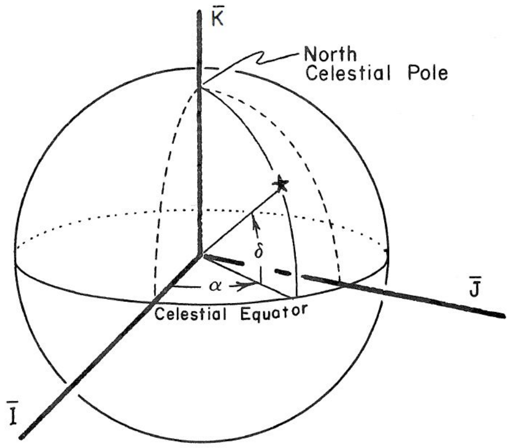

Figure 3.7: Right Ascension - Declination Reference System [17]

This reference frame is related to the Equatorial Coordinate System. Its foundamental plane is the "Celestial Equator", that is the extension of Earth's equatorial plane to a sphere with infinite radius called "celestial sphere". It is a polar coordinate system, so that every object in the celestial sphere can be located by two angles and a distance:

- α is the right ascension and it is measured starting from the Vernal equinox direction and proceeding eastward in the foundamental plane:
- δ is the declination, measured from the celestial equator proceeding nordward;
- r: is the position vector that measures the distance from the origin of the reference frame.

3.4 Classic Orbital Elements

The classical orbital elements are six independent parameters that describe the size, shape, orientation of the orbit and the position of a satellite on that orbit at a precise time [17]. This set is composed by:

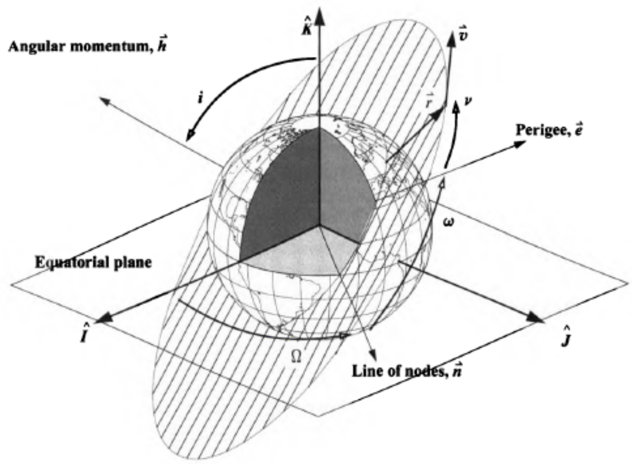

Figure 3.8: Classic Orbital Elements [19]

- a: *semi-major axis* of the trajectory (define the size of the orbit);
- e: *eccentrity* of the conic section (define the shape of the orbit);
- i: *inclination*, defined as the angle between unit vector K and the direction of angular momentum $\vec{h}$;
- Ω: *longitude of the ascending node.* In the foundamental plane is the angle between the unit vector I and the point that cross the foundamental plane in north direction measured counterclockwise. This point is called *ascending node*;
- ω: *argument of periapsis*, or *latitude of the ascending node.* It is the angle between the ascending node and the periapsis, measured in the plane of the orbit in the direction of satellite's motion;
- ν: *true anomaly at the time t.* It is the angle between periapsis and the position of the satellite at considered time. It is measured in the plane of the orbit and in direction of the motion.

3.5 Patched-Conic Approximation

During an interplanetary transfer the spacecraft is mainly subjected to the gravitational force of the Sun. However, when relatively close to other celestial bodies, their gravitational force becomes stronger than the Sun one. During the preliminary mission analysis it is possible to estimate the total ΔV through the '*patched conix approximation*' which allows to ignore the influence of the Sun when the spacecraft

is a great distance from another body, such as the arrival planet.
Each planet has its own *sphere of influence* (SOI), which can be defined as the region of space in which the effect of the planet is predominant over that of the other celestial bodies and whose radius varies according to the distance of the planet from the Sun.

$$r_{SOI} = R\left(\frac{m}{M}\right)^{2/5} \tag{3.19}$$

where:

- R: is the distance between the two bodies;
- m: is the mass of the smaller object;
- M: is the mass of the bigger object (usually Sun or a planet).

Within this sphere, the motion of a body attracted to the planet can be considered unaffected by other celestial bodies. Therefore, during an interplanetary trip, it is possible to divide the space into regions, assigning each its own sphere of influence. When the satellite transits into the sphere of influence of a planet, only the gravitational force between that body and the satellite is considered. Therefore, the study of the motion of the satellite is carried out by exploiting the two-body problem. The difference is that Delta-Vs are the ones that allow capture and evasion from gravitational fields. It is therefore necessary to consider the trajectory as a series of connected conics. For the aim of this thesis the following subdivision is taken into consideration:

- Heliocentric Phase
- Planetocentric Phase

Planet	R_{SOI} [10^5 Km]
Mercury	1.12
Venus	6.16
Earth	9.29
Mars	5.78
Jupiter	482
Saturn	545
Uranus	519
Neptune	868
Pluto	341

Table 3.2: Planetary Spheres of Influence. Data from [20]

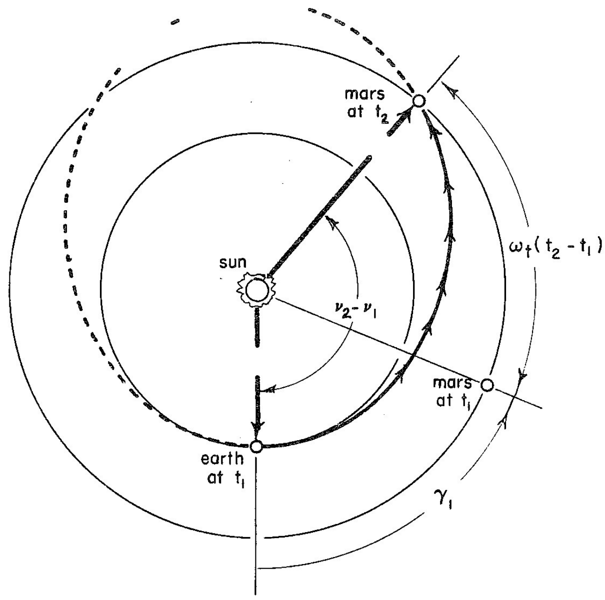

Figure 3.9: Phase angle at departure γ_1 [17]

3.5.1 Heliocentric Phase

The heliocentric phase takes place since the satellite leaves the Earth's sphere of influence and is subject only to the gravitational force of the Sun. Taking an Earth-Mars mission as an example, we must consider not only the arrival on the Martian orbit, but also that the planet has to be right at the point of arrival. We have to study the *phase angle at departure* γ_1 that is the angle between tha radius vectors to the departure and arrival planets [17].

$$\gamma_1 = (\nu_2 - \nu_1) - \omega_t(t_2 - t_1) \tag{3.20}$$

This requirement places limits on launch windows choice. If launch opportunity is missed, the correct phase angle will repeat after a long period, called *Synotic Period* τ_S which depends on the target planets.
To calculate synodic period we made the following considerations:

- the Earth moves through an angle $\omega_\oplus \tau_S$;
- the target planet advances by $\omega_t \tau_S$;
- the original phase angle will be repeated when angular advance of one will exceed that of the other by 2π radians.

We can therefore write the expression in (3.21)

$$\omega_\oplus \tau_S - \omega_t \tau_S = \pm 2\pi \qquad \Rightarrow \qquad \tau_S = \frac{2\pi}{\omega_\oplus - \omega_t} \tag{3.21}$$

Planet	Synodic Period [yr]
Mercury	0.32
Venus	1.60
Mars	2.13
Jupiter	1.09
Saturn	1.04
Uranus	1.01
Neptune	1.01
Pluto	1.00

Table 3.3: Synodic Period of Planets Related to Earth

Table 3.3 collects the data taken from *"Fundamentals of Astrodynamics"* [17] about synodic period of Solar System planets related to Earth. We may concluded that planets very close to the Earth, and therefore with a similar velocity, have long sinodic periods: for Mars is about 2 years. For this reason, if successive launches are considered, this is the waiting time between the possible launches. The eccentricity of Mars changes the arrival V_∞ and this causes there to be more favorable launch windows than others.

Hohmann Transfer

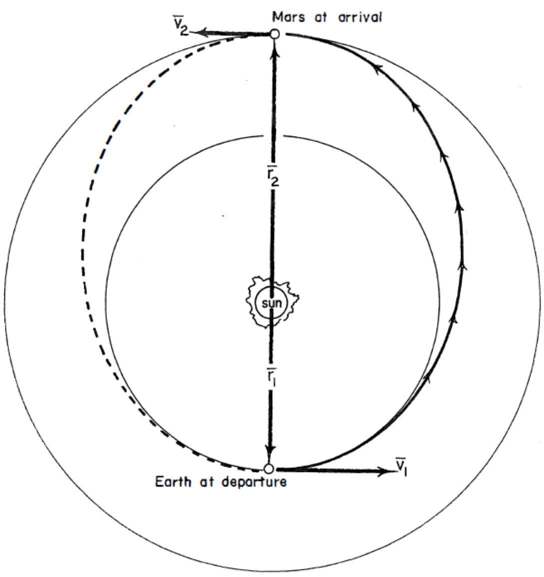

Figure 3.10: A Hohmann transfer from Earth to Mars [17]

For transfers to most of the planets, we may consider that planetary orbits are both circular and coplanar [17].The Hohmann Transfer is the most energy efficient maneuver for circular orbits, but it generally takes long time to be travelled. This transfer orbit is semi-elliptical and tangent to the departure and arrival orbits in the respective apsides: periapsis on the internal circular orbit and apoapsis on the external one.

$$\begin{cases} r_p = r_1 \\ r_a = r_2 \end{cases}$$

The semi-major axis and the eccentricity of the Hohmann trajectory are indicated with a_H and e_H respectively

$$a_H = \frac{r_1 + r_2}{2} \qquad e_H = \frac{r_2 - r_1}{r_1 + r_2} \tag{3.22}$$

Delta-V must be parallel to the velocity, so there are no misalignment losses. Moreover, between circular orbits it is always guaranteed that the flight path angle φ is equal to zero and therefore there are no gravity losses.
As already mentioned, the initial circular orbit velocity is

$$V_{c1} = \sqrt{\frac{\mu}{r_1}} \tag{3.23}$$

while the circular velocity on the arrival orbit is

$$V_{c2} = \sqrt{\frac{\mu}{r_2}} \tag{3.24}$$

As can be seen from the image, the Delta-Vs are linked to the circular velocity of the two orbits and to the velocities V_{H1} and V_{H2}. These relationships can then be written:

$$V_{c1} + \Delta V_1 = V_{H1} \tag{3.25}$$

$$V_{c2} = V_{H2} + \Delta V_2 \tag{3.26}$$

The expressions of the Hohmann maneuver velocities can be obtained with an energy balance, exploiting the equation of the specific mechanical energy:

$$\varepsilon = \frac{\mu}{2a} = \frac{V^2}{2} - \frac{\mu}{r} \tag{3.27}$$

from which derived

$$\varepsilon_H = -\frac{\mu}{2a} = -\frac{\mu}{r_1 + r_2} = \frac{V^2}{2} - \frac{\mu}{r} \tag{3.28}$$

The expression of velocities then becomes:

$$V_{H1} = \sqrt{2\left(-\frac{\mu}{r_1 + r_2} + \frac{\mu}{r_1}\right)} \tag{3.29}$$

$$V_{H2} = \sqrt{2\left(-\frac{\mu}{r_1 + r_2} + \frac{\mu}{r_2}\right)} \tag{3.30}$$

Therefore, the cost of the first maneuver is calculated as:

$$\Delta V_1 = V_{H1} - V_{c1} = V_{c1}\sqrt{\left(\frac{2r_2}{r_1 + r_2} - 1\right)} \tag{3.31}$$

and the cost of the second maneuver:

$$\Delta V_2 = V_{c2} - V_{H2} = V_{c2}\sqrt{\left(1 - \frac{2r_1}{r_1 + r_2}\right)} \tag{3.32}$$

The total cost is given by the sum of the two contributions

$$\Delta V = |\Delta V_1| + |\Delta V_2| \tag{3.33}$$

In the case presented in this master thesis the transfer occurs from an smaller radius orbit to a larger radius orbit, so both Delta-V positive will be positive (acceleration). the cost-effectiveness of this type of manuever is paid for with its duration, which will be half of the transfer orbital period.

$$\Delta T_H = \pi\sqrt{\frac{a_H^3}{\mu}} \tag{3.34}$$

3.5.2 Planetocentric Phase

According to MSR Mission architecture, the spacecraft will perform two maneuvers in Mars' sphere of influence:

- Parking Orbit Capture
- Parking Orbit Escape

The Capture manuever is referred to the passage from the hyperbolic trajectory to the parking orbit, while during the Escape the spacecraft will leave the parking orbit to enter the return hyperbolic trajectory. Both these maneuvers are explained in the following paragraphs.

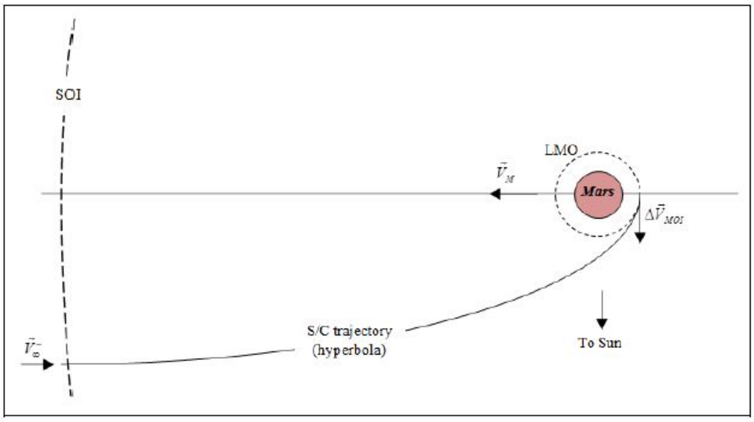

Figure 3.11: Capture Maneuver [21]

Parking Orbit Capture

During the capture maneuver in the Martian SOI, the spacecraft switches from the hyperbolic entry trajectory to the parking orbit. To perform this change, a speed variation is required. To be able to calculate the DeltaV of the maneuver, we need a couple of data:

- Hyperbolic excess velocity V_∞ or the energy level C_3 for capture conditions. These parameters are linked by the following equation:

$$\varepsilon_\infty = \frac{V_\infty^2}{2} = \frac{C_3}{2} \tag{3.35}$$

- Capture Parking Orbit velocity $\vec{V}_{orbit}$.

From the hyperbolic energy equation at a given radius it is possible to derive the hyperbolic velocity:

$$\vec{V}_{hyp} = \sqrt{C_3 + \frac{2\mu}{r}} \tag{3.36}$$

while the expression of the parking orbit velocity, known the geometry parameters, is calculated from the energy equation. The expression is given by (3.37)

$$\vec{V}_{orbit} = \sqrt{\frac{2\mu}{r} - \frac{\mu}{a}} \tag{3.37}$$

Thus, the velocity increment for the capture maneuver is calculated as follows:

$$\Delta V_{capture} = \vec{V}_{orbit} - \vec{V}_{hyp} \tag{3.38}$$

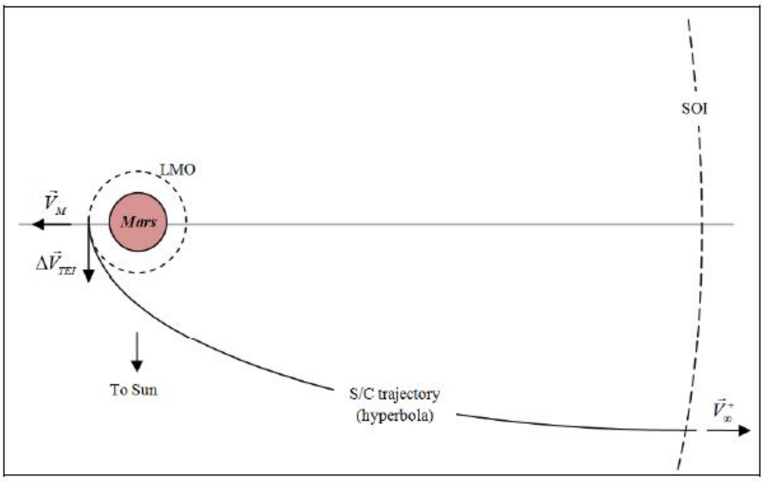

Figure 3.12: Escape Maneuver [21]

Parking Orbit Escape

For the Escape maneuver the reasoning is the same, except that this time the spacecraft passes from the parking orbit to an hyperbolic trajectory. In this case the parameters to know are:

- Hyperbolic excess velocity V_∞ or the energy level C_3 for escape conditions;
- Escape Parking orbit velocity V_{orbit}.

The data can be calculated as the capture condition, considering r the escape radius vector. Thus, the velocity increment is calculated as:

$$\Delta\vec{V}_{escape} = \vec{V}_{hyp} - \vec{V}_{orbit} \tag{3.39}$$

Chapter 4

Parking Orbit Optimization Problem

For an interplanetary mission, such as the one considered in this thesis, the choice of a correct parking orbit is very important. Based on this, in fact, the costs of the mission and the masses will vary, in particular the propellant mass. This thesis analyzes a round trip to Mars for a Sample Return mission. This chapter introduces the computation process used in the MATLAB code, which will exploit the genetic algorithm for the optimization of the problem. The analytical method presented is based on the paper *Optimum Parking Orbit Orientation for a Three-Dimensional Capture-Escape Mission* [22].
The mission has been studied in different configurations, whose detailed descriptions are contained in Chapter 5, but the process described in this Chapter is valid for all of them.

4.1 Assumptions

The assumptions used to study the optimization problem are here described:

- The hypotheses of the two-body problem are considered valid, therefore it is applied to the study of the problem and spacraft can be treated as a point mass;
- Parking orbit can be circular or elliptical and may have any orientation;
- The orientation and energy related to the hyperbolic asymptotes of capture and escape are dependent on the dates of arrival and departure and on the duration of the heliocentric phase
- Each maneuver is characterized by a single-impulsive burn;
- All maneuvers are carried out with chemical propulsion.

4.2 Input and Output

The problem is divided into three different parts, namely capture, determination of the parking orbit and escape. The only gravitational force in the problem is the Mars one, because all phases take place within the Martian sphere of influence.

Parameters		Description
a	$[Km]$	Parking Orbit Semi-major Axis
e		Parking Orbit Eccentricity
i	$[deg]$	Parking Orbit Inclination
$C3_c$	$[Km^2/s^2]$	Capture - Energy Level
α_c	$[deg]$	Capture - Right Ascension
δ_c	$[deg]$	Capture - Declination
$C3_e$	$[Km^2/s^2]$	Escape - Energy Level
α_e	$[deg]$	Escape - Right Ascension
δ_e	$[deg]$	Escape - Declination

Table 4.1: Optimization Problem Input Parameters and Output

Starting from the input data, shown in the previous Table, the algorithm will generate results that refer to:

- the orientation of the parking orbit;
- the capture and escape positions;
- the cost of each maneuver performed;

- the masses related to each maneuver.

The parameters optimized by the algorithm and the outputs of the problem are summarized in the following Table. The inputs and outputs described in this section

Optimized Parameters		Description
ρ_c	$[deg]$	Capture Injection Angle
ρ_e	$[deg]$	Escape Injection Angle
Ω_c	$[deg]$	Capture - Right Ascension of the Ascending Node
Ω_e	$[deg]$	Escape - Right Ascension of the Ascending Node
ω_c	$[deg]$	Capture - Argument of Periapsis
ω_e	$[deg]$	Escape - Argument of Periapsis
Output Parameters		Description
ΔV_c	$[Km/s]$	Capture - Velocity Increment
ΔV_e	$[Km/s]$	Escape - Velocity Increment
ΔV	$[Km/s]$	Total Velocity Increment
M_{total}	$[deg]$	Total Initial Mass

Table 4.2: Optimization Problem Output Parameters

are related to the single launch mission. In this thesis, multiple launch missions have been also optimized. However, the input and output parameters will be essentially the same, in fact will vary only the quantity of these parameters. Any variation of these parameters will however be specified in the missions related Section of Chapter 5

4.3 Resolution Process

The effects of orbit perturbations are neglected in the description of this Section. the parking orbit will have the same orientation for the entire duration of the mission. The calculation process for perturbations is explained in the next Section.

4.3.1 Parking Orbit Definition

The reference frame used for this part is the equatorial system of Mars, therefore it is the same as described in Subection 3.3.2 but with the origin coincident with the center of Mars. The quantities will then be obtained in relation to the IJK axes. It is therefore necessary to take into account the rotations to be performed to carry out the transformation of the variables from the perifocal to the equatorial system. The first step is the introduction of the rotation matrices $[-\Omega]_K$, $[-i]_I$ and $[-\rho_c]_K$, where the minus indicates the inverse matrix and the subscript indicates the axis around which the rotation occurs.

$$[-\Omega]_K = \begin{bmatrix} \cos\Omega & -\sin\Omega & 0 \\ \sin\Omega & \cos\Omega & 0 \\ 0 & 0 & 1 \end{bmatrix} \tag{4.1}$$

$$[-i]_I = \begin{bmatrix} 1 & 0 & 0 \\ 0 & \cos i & -\sin i \\ 0 & \sin i & \cos i \end{bmatrix} \tag{4.2}$$

$$[-\rho_c]_K = \begin{bmatrix} \cos\rho_c & -\sin\rho_c & 0 \\ \sin\rho_c & \cos\rho_c & 0 \\ 0 & 0 & 1 \end{bmatrix} \tag{4.3}$$

It can be now calculated the vector unit along the line of the ascending node, remembering that it is defined only when the plane of the orbit is not zero, otherwise it coincides with the equatorial plane and becomes undefined.

$$\widehat{A} = [-\Omega]_K[-i]_I \begin{bmatrix} 1 \\ 0 \\ 0 \end{bmatrix} \tag{4.4}$$

To define the position of the satellite along the orbit trajectory, is considered the true anomaly ν, which is one of the six orbital elements defined in Section 3.4.

$$\nu = 2\pi + \rho_c - \omega_c \tag{4.5}$$

It is now possible to calculate the magnitude of the position vector r.

$$r = \frac{a(1-e^2)}{1+e\cos\nu} \tag{4.6}$$

The direction of the position vector must be defined through its unit vector $\widehat{r}$, obtained with the rotations described in Equation (4.7),

$$\widehat{r} = [-\Omega]_K[-i]_I[-\rho_c]_K \begin{bmatrix} 1 \\ 0 \\ 0 \end{bmatrix} \tag{4.7}$$

The vector position it is now simple to calculate.

$$\vec{r} = r\widehat{r} \tag{4.8}$$

The next goal is the velocity calculation, which magnitude can be expressed through specific mechanical energy.

$$V = \sqrt{\frac{2\mu}{r} - \frac{\mu}{a}} \tag{4.9}$$

The direction of the speed, on the other hand, must be calculated knowing the flight path angle γ, which requires the specific angular momentum $\vec{h}$

$$\begin{cases} \vec{h} = \vec{r} \times \vec{V} \Rightarrow h = rV \sin\gamma \\ h = \sqrt{\mu a(1-e^2)} \end{cases}$$

$$\gamma = \sin^{-1}\left(\frac{h}{rV}\right) \tag{4.10}$$

In the code used for the optimization, has been inserted a control on this angle value, as the sine is defined in the interval $[-\pi/2, \pi/2]$; it is also linked to the true anomaly.

$$\begin{cases} 0 \leq \gamma \leq \dfrac{\pi}{2} \quad if\ 0 \leq \Big(\rho_c - \omega_c\Big) \leq \pi \\ \\ \dfrac{\pi}{2} < \gamma < \pi \quad if\ \pi < \Big(\rho_c - \omega_c\Big) \leq 2\pi \end{cases}$$

The direction of the velocity can now be derived, and subsequently also the velocity vector.

$$\widehat{V} = [-\Omega]_K[-i]_I[-\rho_c]_K[-\gamma]_K \begin{bmatrix} 1 \\ 0 \\ 0 \end{bmatrix} \tag{4.11}$$

$$\vec{V} = \widehat{V} V \tag{4.12}$$

where:

$$[-\gamma]_K = \begin{bmatrix} \cos\gamma & -\sin\gamma & 0 \\ \sin\gamma & \cos\gamma & 0 \\ 0 & 0 & 1 \end{bmatrix} \tag{4.13}$$

4.3.2 Capture and Escape Conditions

After the determination of the position and velocity related to the parking orbit, it is possible to obtain the conditions of capture and escape. The input data useful in this phase are those relating to the hyperbolic energy level $C3$, and the right ascension α and declination δ values. From the first, it can be easily obtained the magnitude of the hyperbolic excess velocity V_∞, while from the other two the direction of the hyperbolic asymptote $\widehat{S}$

$$V_\infty^2 = C3 \tag{4.14}$$

$$\widehat{S} = [-\alpha]_K[\delta]_J \begin{bmatrix} 1 \\ 0 \\ 0 \end{bmatrix} \tag{4.15}$$

with the rotation matrix expressed as:

$$[-\alpha]_K = \begin{bmatrix} \cos\alpha & -\sin\alpha & 0 \\ \sin\alpha & \cos\alpha & 0 \\ 0 & 0 & 1 \end{bmatrix} \tag{4.16}$$

$$[\delta]_J = \begin{bmatrix} \cos\delta & 0 & \sin\delta \\ 0 & 1 & 0 \\ -\sin\delta & 0 & \cos\delta \end{bmatrix} \tag{4.17}$$

The discussion is now divided for the two capture and escape conditions.

Capture Condition

To define the transition between the hyperbolic orbit and the stopover orbit, two angles are defined, which measure the rotation between the position vector (fixed) and the hyperbolic asymptote, and are considered positive if the measurement is performed in the direction of motion from $\widehat{S}$ to $\widehat{r}$.

$$\beta_1 = \cos^{-1}\left(\frac{\widehat{S}\ \widehat{r}}{|\widehat{S}||\widehat{r}|}\right) \tag{4.18}$$

$$\beta_2 = 2\pi - \cos^{-1}\left(\frac{\widehat{S}\ \widehat{r}}{|\widehat{S}||\widehat{r}|}\right) \tag{4.19}$$

From this can be deduced that there are two possible hyperbolas, with different eccentricity, that can be considered for insertion into orbit. One of the hyperbolas will follow a direct motion, while the other a reverse motion. To understand the direction of motion, the unit vector of the angular momentum has to be obtained.

$$\widehat{W_h} = \frac{\widehat{S} \times \widehat{r}}{\sin\beta} \tag{4.20}$$

If the product of the angular momentum unit vector and K-axis is positive then the motion is direct, otherwise it will be retrograde.
The orientation of the hyperbola remains to be studied. To do this, the true anomaly, the position of the periapsis and the hyperbolic eccentricity have to be determined. First, the tangent of the angle between the periapsis and the hyperbolic asymptote Φ_A is calculated as follows:

$$\sigma = \frac{C3_c r}{2\mu} \tag{4.21}$$

$$\tan\Phi_A = \sigma\sin\beta + \sqrt{(1+\sigma)^2 - (1+\sigma\cos\beta)^2} \tag{4.22}$$

Now it is possible to write the relation that defines the hyperbolic eccentricity, and, subsequently, the value of Φ_A.

$$e_h = \sqrt{\tan^2 \Phi_A + 1} \tag{4.23}$$

$$\Phi_A = \cos^{-1}\left(-\frac{1}{e_h} \right) \tag{4.24}$$

The inverse tangent function is defined in the interval $[-\pi/2, \pi/2]$, but β goes from 0 to 2π, so to verify it is possible to reverse Equation (4.22).
The last quantity to be obtained is the true anomaly that indicates the position of the spacecraft with respect to the periapsis of the hyperbola, whose direction is defined by Φ_A.

$$\nu_{hyp} = \Phi_A - \beta \tag{4.25}$$

It is now possible to derive the hyperbolic velocity vector, whose magnitude is derived from specific energy equation. The equation is applied in two different points, the first is the maneuver position while the other is set to infinite distance.

$$V_h = \sqrt{\frac{2\mu}{r} + C3} \tag{4.26}$$

The velocity unit vector can be obtained from the following expression:

$$\widehat{V_h} = \hat{r}\cos\gamma_h + (\widehat{W} \times \hat{r})\sin\gamma_h \tag{4.27}$$

The γ_h angle is determined, as described in the previous section, through the evaluation of the angular momentum.

$$\begin{cases} \vec{h}_h = \vec{r} \times \vec{V}_h \Rightarrow h = rV_h \sin\gamma_h \\ h_h = \mu\sqrt{\dfrac{e_h^2 - 1}{C3}} \end{cases}$$

$$\gamma_h = sin^{-1}\left(\frac{h_h}{rV_h}\right) \tag{4.28}$$

Also in this case some considerations on the γ_h angle will have to be made. In fact, the injection can be performed on the incoming or outcoming leg, and this depends on the value of the Φ angle.

$$\begin{cases} 0 \leq \gamma_h \leq \pi/2 \quad if\ 0 \leq \Phi \leq -pi \\ \pi/2 < \gamma_h < \pi \quad if\ \pi < \Phi\ 2\pi \end{cases}$$

Before calculating the velocity vector, it is necessary to verify that the result of the Equation (4.6) coincides with that of the position calculated with the following expression:

$$r_h = \frac{a_h(e_h^2 - 1)}{1 + e_h \cos \nu_{hyp}} \tag{4.29}$$

with a_h the semi-major axis of the hyperbola.

$$a_h = \frac{\mu}{C3} \tag{4.30}$$

Finally, the velocity vector is obtained.

$$V_h = V_h \widehat{V_h} \tag{4.31}$$

Escape Condition

To derive position and velocity related to the escape condition, the process remains the same as described for the capture, however some conventions will vary. Therefore, starting from the inputs relating to the exit conditions (C3, right ascension and declination), the β angles are obtained, but this time positive if measured in the direction of motion from r to $\widehat{S}$ along the escape hyperbola.

$$\beta_1 = \cos^{-1}\left(\frac{\widehat{r}\ \widehat{S}}{|\widehat{r}||\widehat{S}|}\right) \tag{4.32}$$

$$\beta_2 = 2\pi - \cos^{-1}\left(\frac{\widehat{r}\ \widehat{S}}{|\widehat{r}||\widehat{S}|}\right) \tag{4.33}$$

To distinguish which of the two hyperbolas follows a direct motion and which one follows a retrograde one, the unit vector of the angular momentum have to be written. Then if the product between $\widehat{W_h}$ and the unit vector $\widehat{K}$ is positive, hyperbola's motion is direct, otherwise it is retrograde.

$$\widehat{W_h} = \frac{(\widehat{r} \times \widehat{S})}{\sin \beta} \tag{4.34}$$

For the calculation of the true anomaly, the process remains identical to that of capture. What varies is the expression of $\tan \Phi_A$.

$$\sigma = \frac{C3_c r}{2\mu} \tag{4.35}$$

$$\tan \Phi_A = -\sigma \sin \beta - \sqrt{(1+\sigma)^2 - (1 + \sigma \cos \beta)^2} \tag{4.36}$$

$$e_h = \sqrt{\tan^2 \Phi_A + 1} \tag{4.37}$$

$$\Phi_A = \cos^{-1}\left(-\frac{1}{e_h}\right) \tag{4.38}$$

$$\nu_{hyp} = \Phi_A - \beta \tag{4.39}$$

As for the definition and calculation of the γ_h angle, please refer to the paragraph related to the capture conditions because the process is identical and is therefore not reported. The Equations (4.26) and (4.27) for the magnitude and the direction of velocity remain also valid. Finally, applying the Equation (4.31), escape velocity vector is determined.

4.3.3 Total Velocity Increments

The variation of total velocity, as already explained, will be the sum of the cost due to the capture and that related to the escape. These two contributions will be calculated knowing the velocities related to the parking orbit and the two hyperbolas, and will have expression:

$$\Delta V_c = \sqrt{V_{hc}^2 + V_c^2 - 2V_{hc}V_c\left(\widehat{V}_{hc}\widehat{V}_c\right)} \tag{4.40}$$

$$\Delta V_e = \sqrt{V_{he}^2 + V_e^2 - 2V_{he}V_e\left(\widehat{V}_{he}\widehat{V}_e\right)} \tag{4.41}$$

As a result, the total Delta-V will be

$$\Delta V = \Delta V_c + \Delta V_e \tag{4.42}$$

4.4 Perturbations

The influence of a planet's non-sphericity changes the orientation of the orbit. The ellipsoid that approximates the surface of the planet will have an equation that contains many coefficients, called *harmonics*. The most interesting harmonic from this point of view is J_2, which considers the effect of the flattening of the poles. The two main effects that the perturbations cause are:

- the *nodal regression*, which causes a displacement of the nodes line around the equator in the opposite direction to the satellite's motion; this effect acts on the argument of periapsis ω
- the *apsidal precession*, which causes the gradual rotation of the line that connect the apsides around the main focus in the direction of satellite's motion. The effect is a variation of Ω

The variations of these two quantities will be assessable through their derivatives, which expression is:

$$\dot{\omega} = \frac{3}{2} J_2 \tau \left(\frac{R_{Mars}}{p_{orbit}} \right)^2 \left(2 - \frac{5}{2} \sin^2 i_{orbit} \right) \tag{4.43}$$

$$\dot{\Omega} = -\frac{3}{2} J_2 \tau \left(\frac{R_{Mars}}{p_{orbit}} \right)^2 \cos i_{orbit} \tag{4.44}$$

where:

- $J_2 = 1{,}9595 \cdot 10^{-3}$
- $\tau = \sqrt{\frac{\mu}{a^3}}$
- $R_{Mars} = 3389{,}5 Km$
- $p_{orbit} = a(1 - e^2)$
- $\mu = 42828 \frac{Km^2}{s^2}$

Then, to find the values of ω and Ω in escape conditions it is possible to write:

$$\omega_e = \omega_c + \dot{\omega} t \tag{4.45}$$

$$\Omega_e = \Omega_c + \dot{\Omega} t \tag{4.46}$$

in which t is the mission duration in seconds.
For short mission periods $\Delta t \sim 0$ the Ω and ω variations due to perturbations are negligible.In this case the values of these quantities will be the same for the capture and escape conditions.
However, mission times considered for this thesis are very extended and therefore the calculation of the perturbations is necessary to have a better estimation of the total costs.

4.5 Masses Calculation

This section presents the calculation methods used to determine the masses for each stage of the mission. The mass denomination used for this thesis is as follows:

- m_i is the mass at the beginning of a maneuver;
- m_u is the payload mass, which is the mass at the end of the considered maneuver;

- m_p is the propellant mass needed to perform the entire maneuver;
- m_s represents the structure mass. It is consider as the 10% of the propellant mass.

The following expression is always valid and has been used as a check of the results obtained in Chapter 5:

$$m_i = m_u + m_p + m_s \tag{4.47}$$

The input data for these maneuvers are written below, but will be specified in Section 5.1:

- m_u: payload mass for each maneuver;
- a: semi-major axis of the orbit;
- e: eccentricity of the orbit;
- R_{Mars}: Mars radius;
- μ: Mars gravitational parameter;
- I_{sp}: Specific Impulse, needed to estimate *exhaust gas velocity* $c = \dfrac{I_{sp}}{g_0}$;
- ΔV_c and ΔV_e: velocity increments for capture and escape, which have been already calculated.

The calculation procedure is now shown for each maneuver: ascent, descent, return and arrival.

Ascent

The first maneuver to be considered is the ascent. This maneuver is performed by the Mars Ascent Vehicle (MAV) to bring the samples collected by the Sample Fetch Rover (SFR) into orbit. A Hohmann transfer is considered to pass from the surface of Mars to the parking orbit.
The first step is to calculate the energy associated to the parking orbit and the related velocity, here called V_2:

$$r_p = a(1 - e) \tag{4.48}$$

$$\epsilon = -\frac{\mu}{2a} \tag{4.49}$$

$$V_2 = \sqrt{2\epsilon + \frac{\mu}{r_p}} \tag{4.50}$$

The energy of the Hohmann trajectory and the velocities in the two apsis, defined here as V_0 and V_1, are then calculated.

$$a_H = \frac{r_p + R_{Mars}}{2} \tag{4.51}$$

$$\epsilon_H = -\frac{\mu}{2a_H} \tag{4.52}$$

$$V_1 = \sqrt{2\epsilon_H + \frac{\mu}{R_{Mars}}} \tag{4.53}$$

$$V_0 = \sqrt{2\epsilon_H + \frac{\mu}{r_p}} \tag{4.54}$$

The total cost of the ascent will be the sum of the impulses given at the beginning of the maneuver on the Martian soil and that given to the periapsis to enter the parking orbit. Losses due to misalignment are taken into account by multiplying V_0 by a corrective factor.

$$\Delta V = V_2 - V_1 \tag{4.55}$$

$$\Delta V_{ascent} = 1{,}1V_0 + \Delta V \tag{4.56}$$

The initial mass can now be calculated as:

$$m_i(ascent) = \frac{m_u(ascent)}{\left(e^{-\frac{\Delta V_{ascent}}{c}} - 0{,}1 + 0{,}1e^{-\frac{\Delta V_{ascent}}{c}}\right)} \tag{4.57}$$

Considering Equation 4.47 for the specific maneuver, it becomes:

$$m_i(ascent) = m_u(ascent) + m_p(ascent) + m_s(ascent) \tag{4.58}$$

Having estimated the structural mass at 10% of the mass of the propellant, can be written:

$$m_s(ascent) = 0{,}1m_p(ascent) \tag{4.59}$$

$$m_p(ascent) = \frac{m_i(ascent) - m_u(ascent)}{1{,}1} \tag{4.60}$$

Descent

As for the descent, we consider a Hohmann transfer that begins at the periapsis of the stopover orbit and ends with the landing on the planet. The process is similar to that of the ascent and, therefore, is omitted. The only difference is that the total cost will be given only by the contribution (breaking) given at the start of the maneuver.

$$\Delta V_{descent} = V_2 - V_1 \tag{4.61}$$

$$m_i(descent) = \frac{m_u(descent)}{\left(e^{-\frac{\Delta V_{descent}}{c}} - 0{,}1 + 0{,}1e^{-\frac{\Delta V_{descent}}{c}}\right)} \tag{4.62}$$

$$m_i(descent) = m_u(descent) + m_p(descent) + m_s(descent) \tag{4.63}$$

$$m_s(descent) = 0{,}1m_p(descent) \tag{4.64}$$

$$m_p(descent) = \frac{m_i(descent) - m_u(descent)}{1{,}1} \tag{4.65}$$

Return

This maneuver is related to the transition from the parking orbit around Mars to the hyperbolic trajectory that will bring the spacecraft back to Earth. The cost of the escape maneuver is already known from the calculations made previously, so it can be written:

$$m_i(return) = \frac{m_u(return)}{\left(e^{-\frac{\Delta V_e}{c}} - 0{,}1 + 0{,}1e^{-\frac{\Delta V_e}{c}}\right)} \tag{4.66}$$

$$m_i(return) = m_u(return) + m_p(return) + m_s(return) \tag{4.67}$$

$$m_s(return) = 0{,}1m_p(return) \tag{4.68}$$

$$m_p(return) = \frac{m_i(return) - m_u(return)}{1{,}1} \tag{4.69}$$

Arrival

This is the first maneuver to be carried out by the spacecraft. There is the passage from the hyperbolic trajectory of capture to the stopover orbit. Considering the maneuver cost already calculated ΔV_c, can be written that:

$$m_i(arrival) = \frac{m_u(arrival)}{\left(e^{-\frac{\Delta V_c}{c}} - 0{,}1 + 0{,}1e^{-\frac{\Delta V_c}{c}}\right)} \tag{4.70}$$

$$m_i(arrival) = m_u(arrival) + m_p(arrival) + m_s(arrival) \tag{4.71}$$

$$m_s(arrival) = 0{,}1m_p(arrival) \tag{4.72}$$

$$m_p(arrival) = \frac{m_i(arrival) - m_u(arrival)}{1{,}1} \tag{4.73}$$

4.6 Algorithm Implementation

For the optimization process, reference is made to the MATLAB toolbox called *Global Optimization Toolbox*, which contains the solver *ga* for the use of the genetic algorithm. It was decided to minimize the total mass as it guarantees a more effective solution than the Delta-V minimization. By optimizing the initial mass of arrival, in fact, the algorithm allows to save more on capture costs, in which the masses are highest.
The variables on which the algorithm acts to minimize the total mass are:

- Argument of Periapsis of the parking orbit ω;
- Right Ascension of the Ascending Node Ω;
- Injection Capture ρ_c;
- Injection Escape ρ_e.

The options of *optimoptions*[1] function used for this thesis are:

- `SelectionFcn`: Selection Tournament;
- `EliteCount`: 5;
- `CrossoverFraction`: 0.2;
- `InitialPopulationRange`: $[0; 2\pi]$.
- `MigrationDirection`: both.

[1]for the meaning of the various options described, see the section 2.8

Chapter 5

Results

In this Chapter have been exposed the results of the analyzes carried out with the developed MATLAB code considering different case studies. The Chapter begins with a section on the presentation of input data; after this brief introduction, the results of the analyzes have been presented together with the comparison between different mission configuration, in order to estimate the best concept in terms of initial mass. In the final sections have been highlighted the effects of a variation of semi-major axis and return payload mass on the mission performances.
Before the analyzes, the MATLAB code has been validated comparing obtained results with that of the paper *'Optimum Parking Orbit Orientation for a Three-Dimensional Capture-Escape Mission'* [22].[1]

[1] V.Appendix A

5.1 Input Data

Many variables have been taken in consideration for the optimization problem, considering also space vehicle mass. An eccentric 1-sol parking orbit[2] has been used for all the analyzes, with a semi-major axis equal to 20,448 km, an eccentricity of 0.8 and an inclination of 40 degrees.
Some parameters still remain to be defined:

- Payload mass of return maneuver, m_u *return*, has been set to $200Kg$;
- Payload mass of ascent maneuver, m_u *ascent*, considering a mass structure margin, is $50Kg$;
- Landed Mass, m_u *descent*, is composed by the initial mass of the ascent phase, m_i *ascent* plus the mass that will remain on the planet (rover, structures, MAV launcher ecc ...) that has been estimated to be about $900Kg$;
- Payload mass upon arrival at Mars m_u *arrival* calculated as sum of the initial mass of landing maneuver and initial mass of return maneuver;
- Specific Impulse I_{sp} for capture and escape maneuvers has been set to 450 seconds, assuming to use LOX/LH2 propellant;
- Specific Impulse I_{sp} for MAV ascent maneuver is 300 seconds.

Parking Orbit parameters		Masses input	
semi-major axis a $[Km]$	20448	m_u *return* $[Kg]$	200
eccentricity e	0.8	m_u *ascent* $[Kg]$	50
inclination i $[deg]$	40	m_u *descent* $[Kg]$	900+m_i *ascent*
		m_u *arrival* $[Kg]$	m_i *descent*+m_i *return*

Table 5.1: Input Data

Regarding the capture and escape dates, has been decided to study a possible 2041 Mars Sample Return mission with the data taken from the paper *"Optimizing Parking Orbits for Roundtrip Mars Missions"* [23] and listed in Table5.2.In particular, referring to the MSR mission architecture in Section 1.3, 'Sample Retrieval Lander' and 'Earth Return Orbiter' missions have been chosen for the analyzes of this master thesis.

[2]Sol is used to denote the length of the Martian solar day, that lasts about 24 h, 39 min, 45 sec, for a total of 88775 seconds.

These two missions have been studied through the MATLAB code in different configurations:

- Single Launch: SRL and ERO are treated as a single spacecraft;
- Multiple Launch: SRL and ERO are two distinct entities and they perform two different missions with different parking orbit orientation and launch dates. To understand how to deal with this study, it is necessary to analyze the problem starting from the simplest case. All these steps are detailed in the following sections.

Mars Arrival		Mars Departure	
27/07/2042		31/07/2043	
stay time: 368,7 days			
$V_{\infty}c$ $[Km/sec]$	2,92	$V_{\infty}e$ $[Km/sec]$	2,471
α_c $[deg]$	113,8	α_e $[deg]$	-53,3
δ_c $[deg]$	-1,7	δ_e $[deg]$	5,3

Table 5.2: Input Dates for 2041 Mission

5.2 Single-Launch Configuration

To perform this analysis genetic algorithm optimize four different parameters to minimize the initial mass:

- ω : Argument of Periapsis of the parking orbit;
- Ω : Right Ascension on the Ascending Node of the parking orbit;
- ρ_c : capture injection angle;
- ρ_e : escape injection angle.

Table 5.3 contains the results of the optimization. It contains the subdivision of masses for each maneuver (initial mass, payload mass, propellant consumption and structures). In this way it is simple to verify that the accounts have been made correctly.
For example, it is known that m_u *descent* has to be 900 + m_i *ascent*: from the output data is easily verifiable that 900+636 is actually equal to 1536.
From the results it is clear that between the capture and escape, the latter is much higher in value. This happens because the algorithm, optimizing the initial mass, tends to decrease the capture cost, as it is the one that involves the largest masses.
Looking at the Figure 5.1, it is also possible to evaluate that the algorithm converges quite quickly, in fact the maximum number of iterations has been set at 400 and the convergence occurs before 100 iterations.

Maneuver	m_i $[Kg]$	m_u $[Kg]$	m_p $[Kg]$	m_s $[Kg]$	ΔV $[Km/s]$
Earth-Mars	3777,5	2870,5	824,587	82,4587	1,0872
Descent	2490,6	1536	867,838	86,783	1,2608
Ascent	635,968	50	532,697	53,269	5,3498
Mars-Earth	379,8966	200	163,542	16,3542	2,4852
Total Propellant Mass =2388,66 Kg			$\Delta V_{capt+esc}$=3,5724 Km/s		
Optimized Total Mass =3777,5 Kg			ΔV_{tot}=10,183 Km/s		

Table 5.3: Output data: Single Launch Optimization

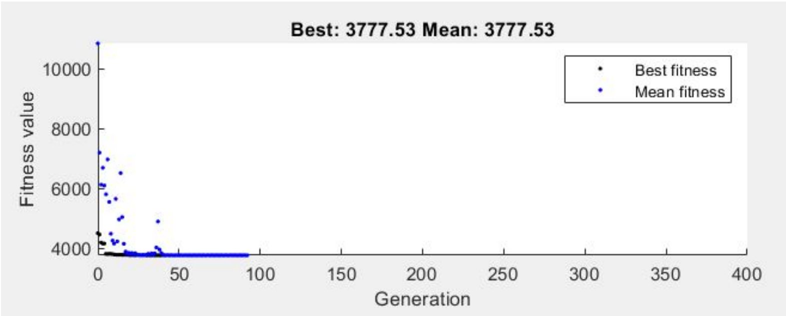

Figure 5.1: Fitness Value - Generation Plot for Single Launch

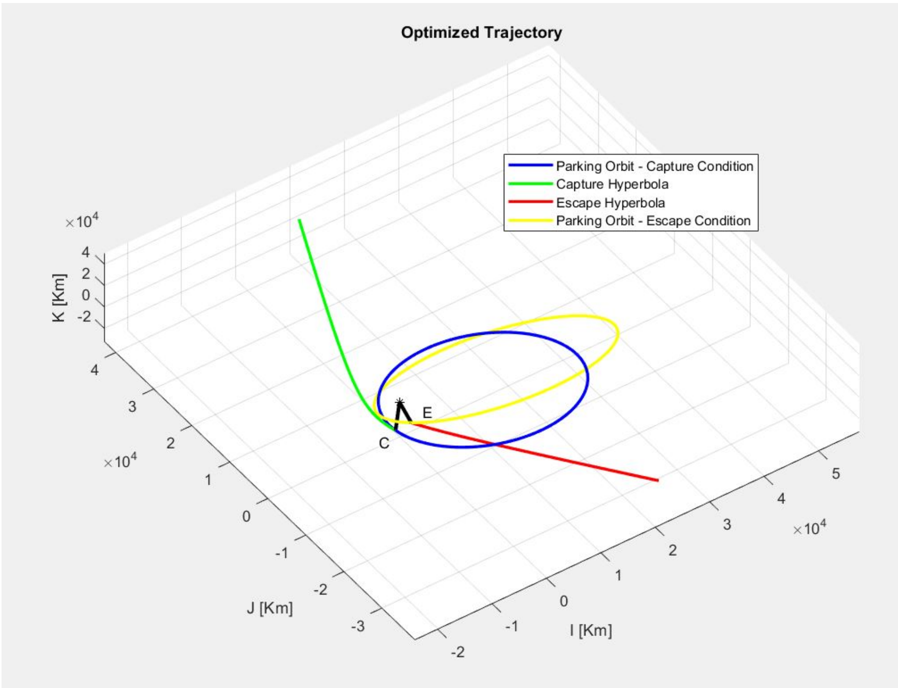

Figure 5.2: 3D Plot for Single Launch

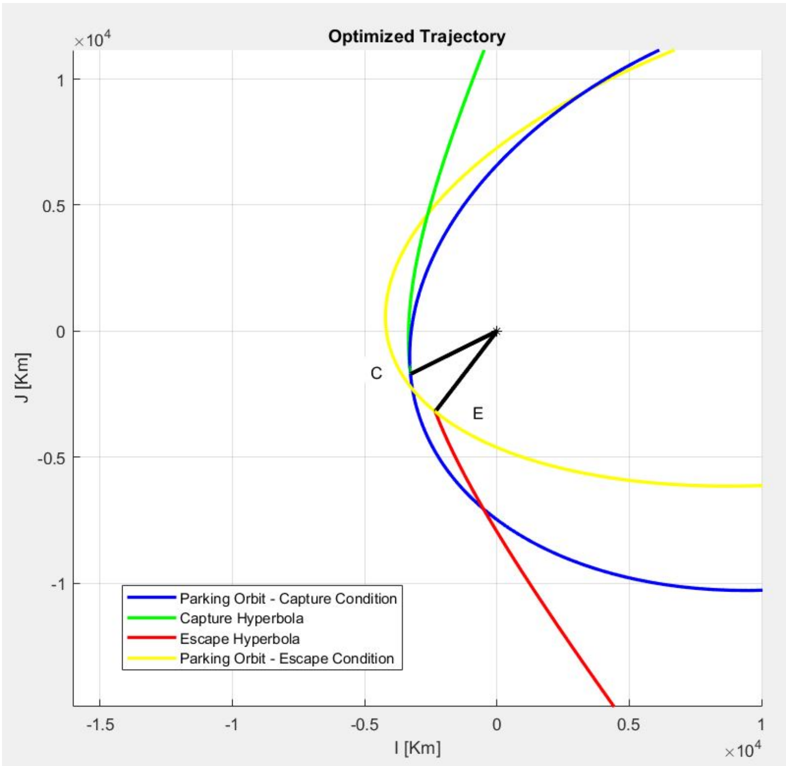

Figure 5.3: Zoom - 3D Plot for Single Launch, I-J view

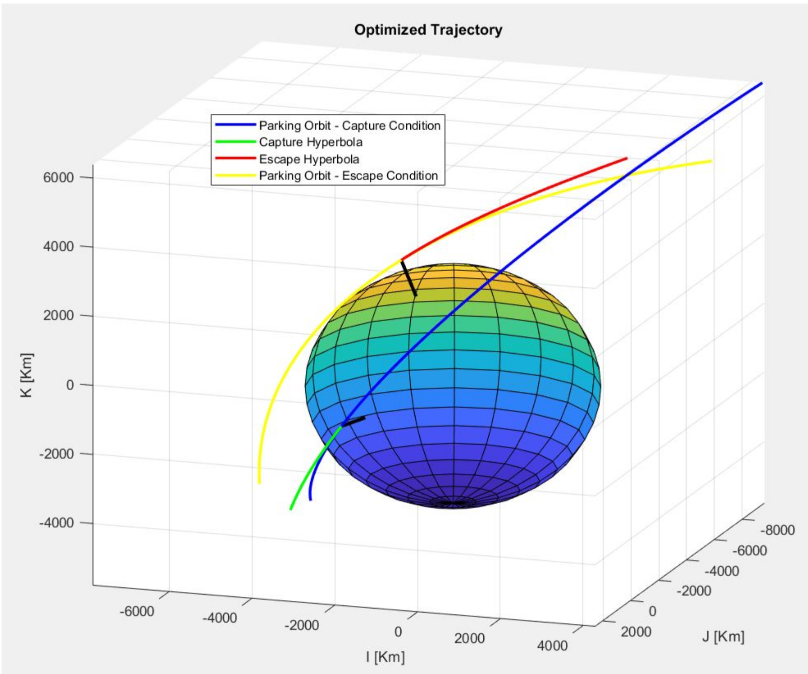

Figure 5.4: Zoom - 3D Plot for Single Launch, Capture and Escape Maneuvers Detail

5.3 Multi-Launch Configuration

In this Section are detailed the analysis that have been studied for this thesis work. They are presented from the simpliest to the most complex, and they are:

- Same Parking Orbit Mission: two spacecraft launched in the same time and in the same parking orbit;
- Different Parking Orbit Mission: two spacecraft launched in the same time but with different optimized parameters;
- Different Dates Mission: two spacecraft launched in different launch windows and with different optimized parameters.

5.3.1 Same Parking Orbits

As the first case for the double launch mission, the configuration chosen provides for a subdivision of the masses: on the one hand, the Lander will have to touchdown on Martian soil and, through the Mars Ascent Vehicle, will bring the samples back to the parking orbit at the end of his mission, and on the other hand there is the Orbiter which will remain on the parking orbit, providing communications with the Earth, and returning the samples received from the MAV in Earth orbit.
The parameters to be optimized remain the same as in the single launch case. By releasing the two masses in this way, an extra relationship is needed to solve the problem, which is the passage of mass that occurs when the samples are moved from the lander to the orbiter for return. So it can be written that the arrival mass of the orbiter at the beginning of return manuver is the same as the arrival on Mars orbit plus the mass of the Orbital Sample (OS) delivered by the MAV. Thus, can be written:

$$m_i \ return_{orbiter} = m_u \ arrival_{orbiter} + m_u ascent_{lander} \tag{5.1}$$

Looking at the data obtained in the Table 5.4, it can be seen that the capture ΔVs of the two spacecraft are identical as both are optimized through the same parameters and therefore they have the same capture hyperbola and the same injection point. For this reason, in the plot of Figure 5.6 there is only one capture trajectory. So, only with a subdivision of the masses there is a small saving in terms of mass compared to the previous case of about 70 Kg. The total Delta-V cost is increased compared to the single launch case, but the cause is the presence of an extra maneuver, due to the mass splitting. Also in this case in the Figure 5.5 the convergence speed of the genetic algorithm can be positively assessed.

Maneuver	m_i $[Kg]$	m_u $[Kg]$	m_p $[Kg]$	m_s $[Kg]$	ΔV $[Km/s]$
			Lander		
Earth-Mars	3277,6	2490,6	715,545	71,545	1,0871
Descent	2490,6	1536	867,8382	86,7838	1,2608
Ascent	635,9674	50	532,6976	53,2698	5,3498
			Orbiter		
Earth-Mars	430,6546	327,2478	94,006	9,4006	1,0871
Mars-Earth	377,2478	200	161,134	16,1134	2,4591
Total Propellant Mass =2371,13 Kg			$\Delta V_{capt+esc}$=4,633 Km/s		
Optimized Total Mass =3708,255 Kg			ΔV_{tot}=11,244 Km/s		

Table 5.4: Output data: Multiple Launch, Same Parking Orbits Optimization

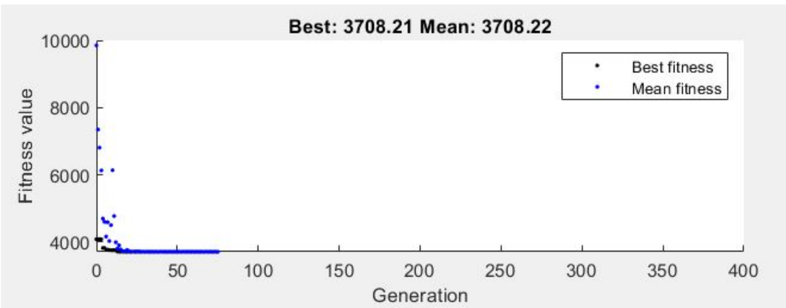

Figure 5.5: Fitness Value - Generation Plot for Multi Launch - Same Orbits

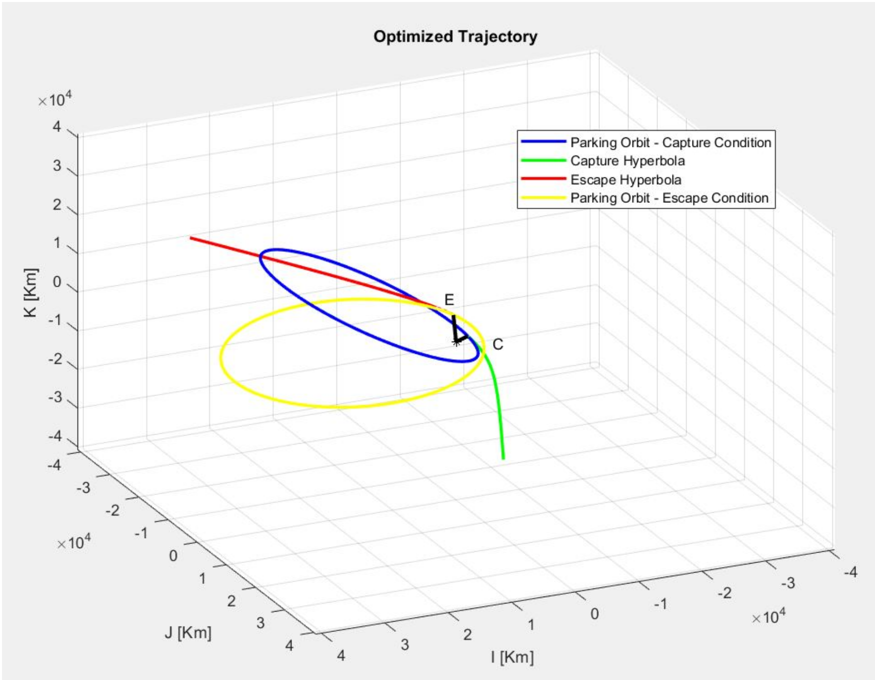

Figure 5.6: 3D Plot for Multi Launch - Same Orbits

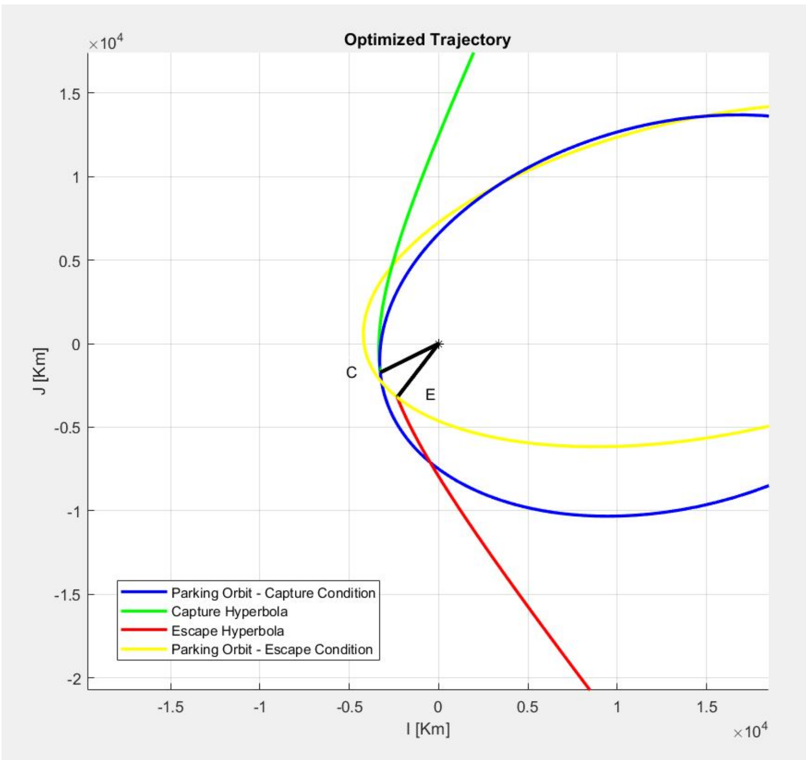

Figure 5.7: Zoom - 3D Plot for Multi Launch - Same Orbits, I-J View

5.3.2 Different Parking Orbits

At this point it is necessary to make the algorithm to optimize different parameters for the two missions. In total there will be seven parameters:

- $\omega_{orbiter}$: Argument of Periapsis of the Orbiter parking orbit;
- $\Omega_{orbiter}$: Right Ascension on the Ascending Node of the Orbiter parking orbit;
- $\rho_{c\ orbiter}$: capture injection angle of the Orbiter;
- $\rho_{e\ orbiter}$: escape injection angle of the Orbiter.
- ω_{lander} : Argument of Periapsis of the Lander parking orbit;
- Ω_{lander} : Right Ascension on the Ascending Node of the Lander parking orbit;
- $\rho_{c\ lander}$: capture injection angle of the Lander;

The results in Table 5.5 show that with two orbits the genetic algorithm can minimize both capture and escape ΔVs. Being lander more massive than the orbiter, the priority is to minimize its ΔV_c value, which in fact is equal to that obtained in the case with same orbits. In that case ga had to decrease both the capture ΔV_c, accepting a higher ΔV_e.By analyzing the masses obtained with the algorithm it can be concluded that, compared to the case with the same orbit, there is a saving on the total mass of about 80 Kg. This saving is completely due to the orbiter, in fact the initial mass of the lander is identical to the case with same parking orbits. This happens because, as just explained, the algorithm, being able to choose two different orbits, is able to minimize the costs, and therefore the mass of the orbiter. Comparing, instead, this configuration with the single launch mission, there is an effective saving in mass, with a saving of about 150 Kg.
ΔV has been decreased by about 0.5 Km/s compared to the case in which the two parking orbits had the same orientation.
Also in this case the optimization is fast in convergence, which occurs just after 100 iterations (Figure 5.8). As for the 3D visualization of the capture and escape phases (from Figure 5.9 to 5.12), it is necessary to have two plots, one relating to the orbiter and one relating to the lander, in which only the capture maneuver is rapresented. Since the Lander has only the capture phase, the algorithm can choose the best insertion point for the maneuver, which is certainly in the periapsis, where the stopover orbit velocity is higher and therefore the speed variation between the capture trajectory and the parking orbit is minimal and the velocities will have minimal misalignment.

Maneuver	m_i $[Kg]$	m_u $[Kg]$	m_p $[Kg]$	m_s $[Kg]$	ΔV $[Km/s]$
			Lander		
Earth-Mars	3277,5	2490,6	715,3747	71,5375	1,0871
Descent	2490,6	1536	867,8382	86,7838	1,2608
Ascent	635,967	50	532,6976	53,2698	5,3498
			Orbiter		
Earth-Mars	350,2986	198,4429	138,05	13,8	2,2134
Mars-Earth	248,443	200	44,04	4,404	0,8628
Total Propellant Mass =2298 Kg			$\Delta V_{capt+esc}$=4,163 Km/s		
Optimized Total Mass =3627,79 Kg			ΔV_{tot}=10,774 Km/s		

Table 5.5: Output data: Multiple Launch, Different Parking Orbit Optimization

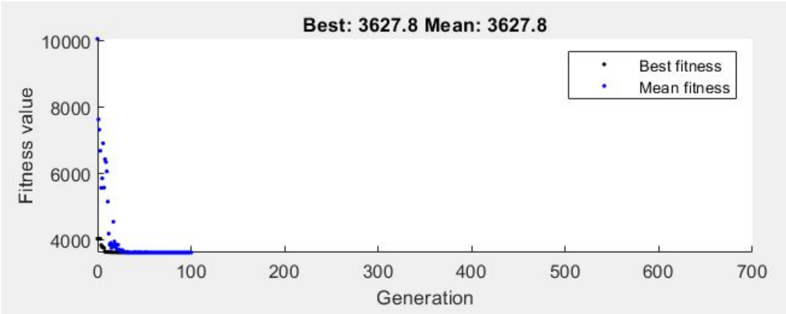

Figure 5.8: Fitness Value - Generation Plot for Multi launch - Different Orbits

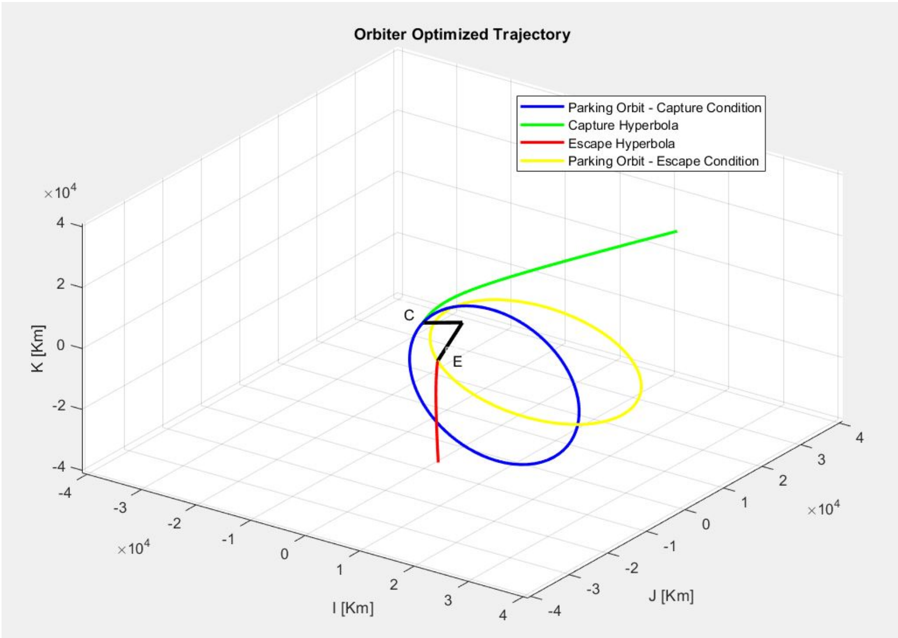

Figure 5.9: 3D Plot for Multi Launch - Different Orbits , Orbiter

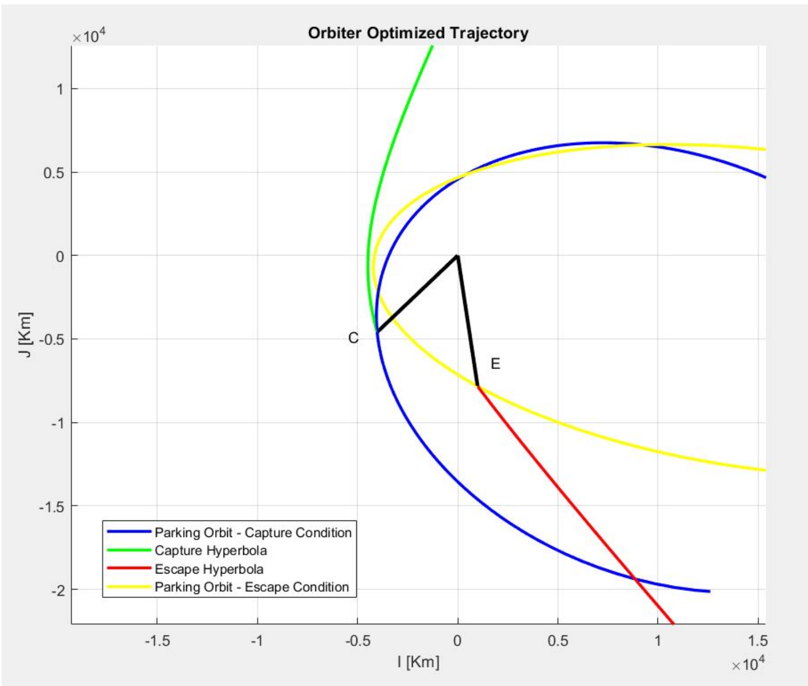

Figure 5.10: Zoom - 3D Plot for Multi Launch - Different Orbits , Orbiter, I-J View

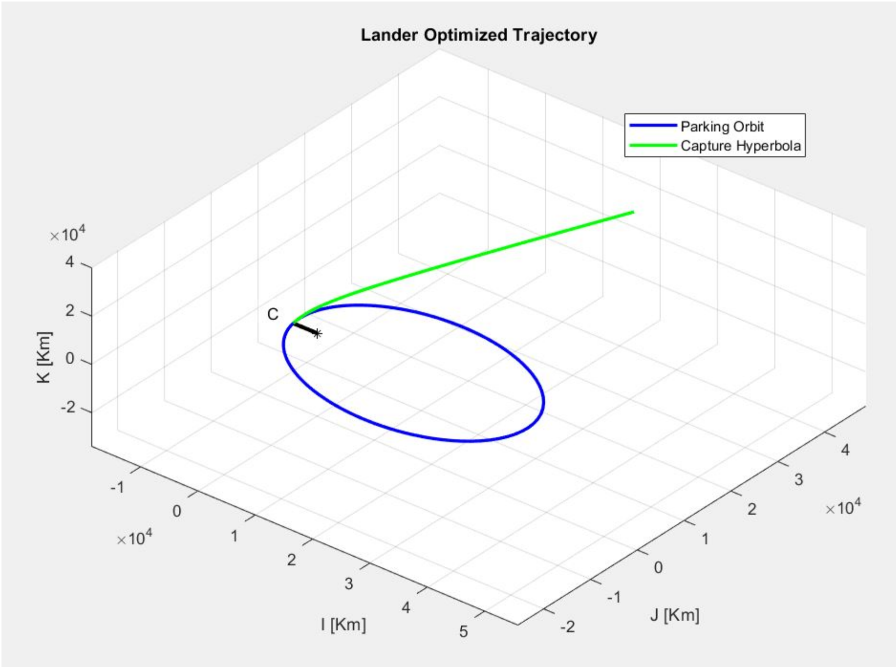

Figure 5.11: 3D Plot for Multi Launch - Different Orbits , Lander

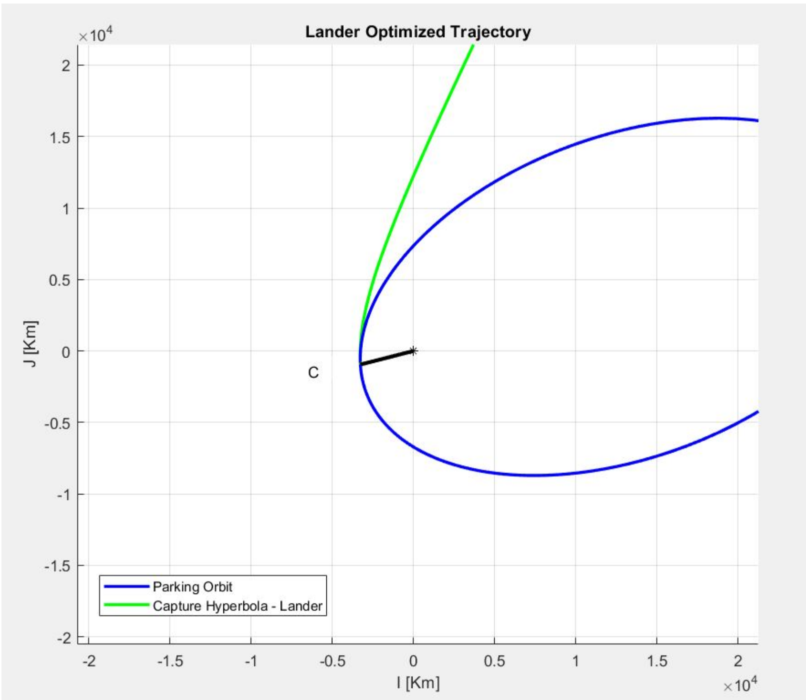

Figure 5.12: Zoom - 3D Plot for Multi Launch - Different Orbits , Lander, I-J View

5.3.3 Different Launch Dates

To simulate a possible changing in the mission, have been evaluated different launch dates. The first launch window taken into consideration is that of 2039 [24] , which sees the departure of the Lander. Subsequently, in 2041, the Orbiter will be launched from Earth. The lander will have time until 2043 to carry out its mission to collect and deliver the samples to the ERO [23].

Orbiter				Lander	
Mars Arrival 27/07/2042		Mars Departure 31/07/2043		Mars Arrival 09/07/2040	
stay time: 368,7 days				stay time: 1117 days	
$V_\infty c$ $[Km/sec]$	2,92	$V_\infty e$ $[Km/sec]$	2,47	$V_\infty c$ $[Km/sec]$	2,7
α_c $[deg]$	113,8	α_e $[deg]$	-53,5	α_c $[deg]$	94,4
δ_c $[deg]$	-1,7	δ_e $[deg]$	5,3	δ_c $[deg]$	18,7

Table 5.6: Input Dates for the Different Launch Dates Mission

The convergence of the algorithm is very fast also in this case, in fact already after about 100 iteration the process is completed.
Interpreting the results in Table 5.7 it is clear that the costs of capture and escape of the orbiter are very low in terms of propellant consumption. For the lander there is a decrease in the cost of the capture maneuver, compared with the previous configuration, mainly due to the morevfavorable conditions of the capture in 2039, in particular for $V_\infty c$. Then, the Total Delta-V decrease because there are more advantageous conditions for the return (smaller $V_\infty e$). The total mass is decreased by about 90 Kg compared to the case in which the spacecraft are launched in the same launch window.
Finally, comparing this mission and the single launch one, it can be seen that actually the mass savings goes up to about 242 Kg.
This is mainly due to conditions due to the data of the two launch windows, that, in this case, made the advantages of the two-launch configuration even greater, as $C3$ for the lander arrival in 2040 is smaller compared to the 2042 value.
To better compare the missions it is more correct to refer to the case with distinct orbits because in that way we have the same conditions of departure and arrival and therefore it makes sense to make a comparison. The case presented here, with different launch windows, can be more or less advantageous depending on the dates chosen for the two launches; thus, it is a valid method to compare the effects of different launch windows for multiple launch missions.

Maneuver	m_i $[Kg]$	m_u $[Kg]$	m_p $[Kg]$	m_s $[Kg]$	ΔV $[Km/s]$
			Lander		
Earth-Mars	3182,8	2490,6	629,273	62,927	0,9726
Descent	2490,6	1536	867,8382	86,7838	1,2608
Ascent	635,9674	50	532,6976	53,2698	5,3498
			Orbiter		
Earth-Mars	350,45	198,48	138,15	13,815	2,241
Mars-Earth	248,5	200	44	4,4	0,8607
Total Propellant Mass =2212 Kg			$\Delta V_{capt+esc}$=4,074 Km/s		
Optimized Total Mass =3533,24 Kg			ΔV_{tot}=10,684 Km/s		

Table 5.7: Output data: Multiple Launch, Different Launch Dates Mission Optimization

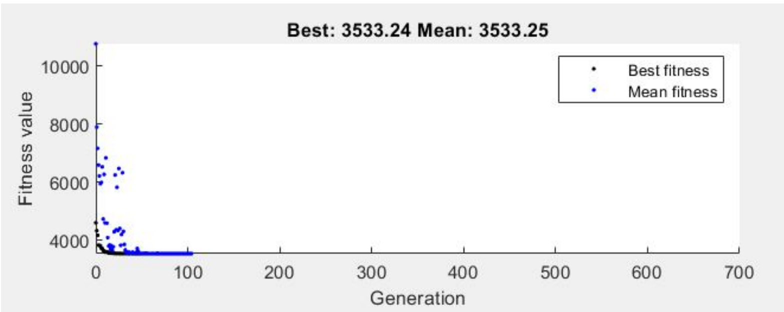

Figure 5.13: Fitness Value - Generation Plot for Multi Launch - Different Launch Mission

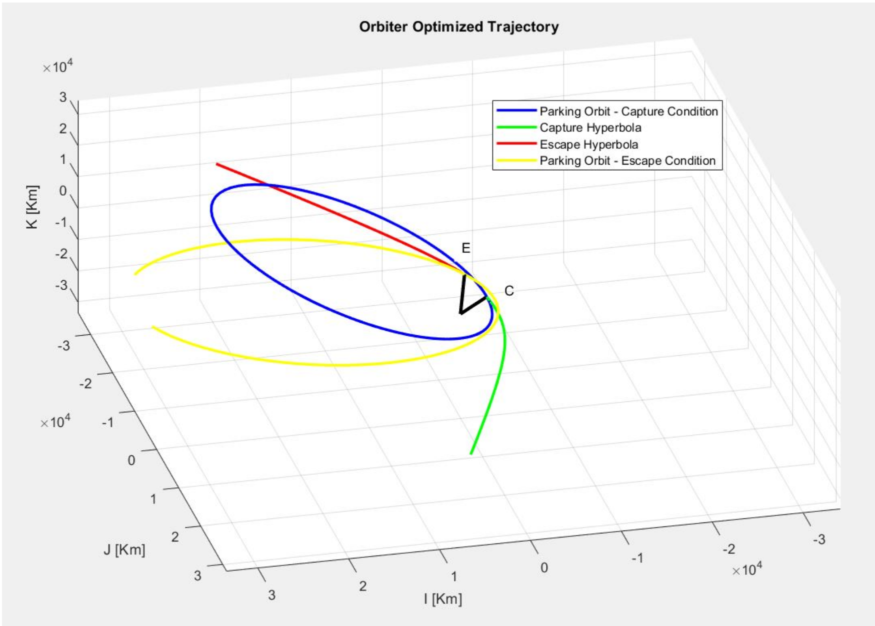

Figure 5.14: 3D Plot for Multi Launch - Different Launch Dates Mission, Orbiter

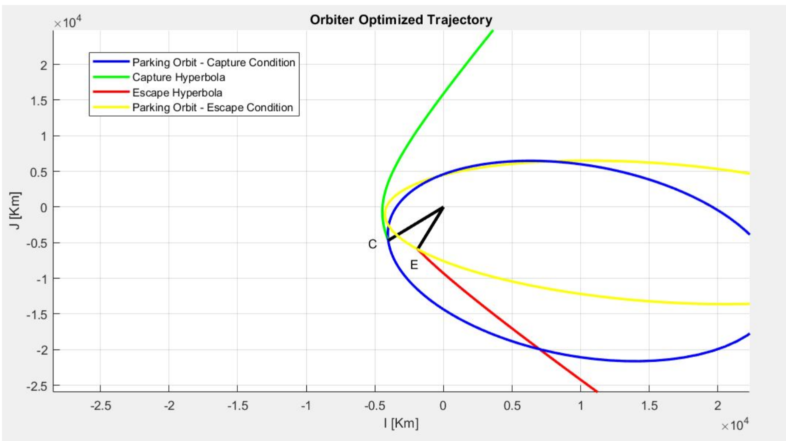

Figure 5.15: Zoom - 3D Plot for Multi Launch - Different Launch Dates Mission, Orbiter, I-J View

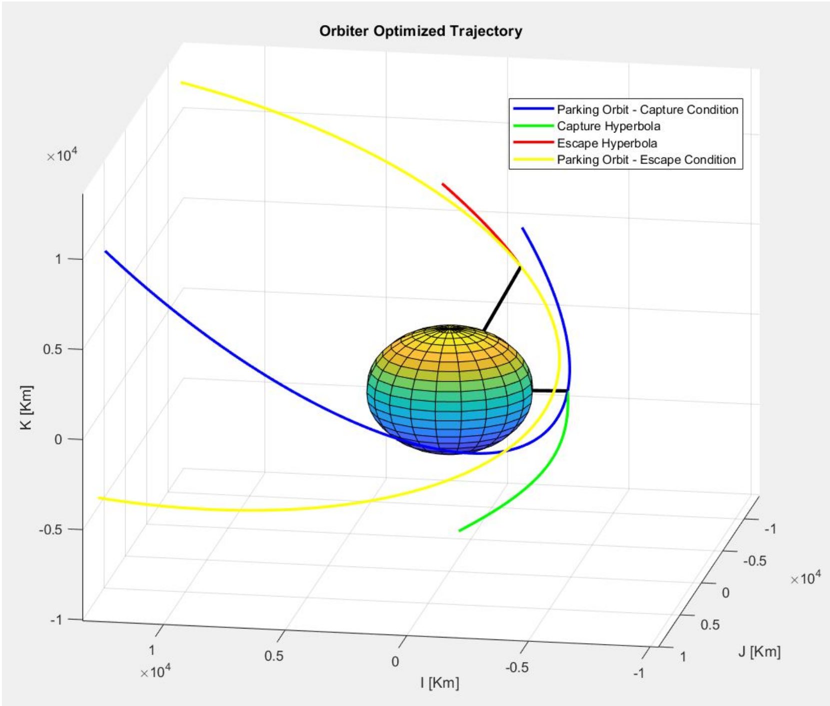

Figure 5.16: Zoom - 3D Plot for Multi Launch - Different Launch Dates Mission, Orbiter, Capture and Escape Detail

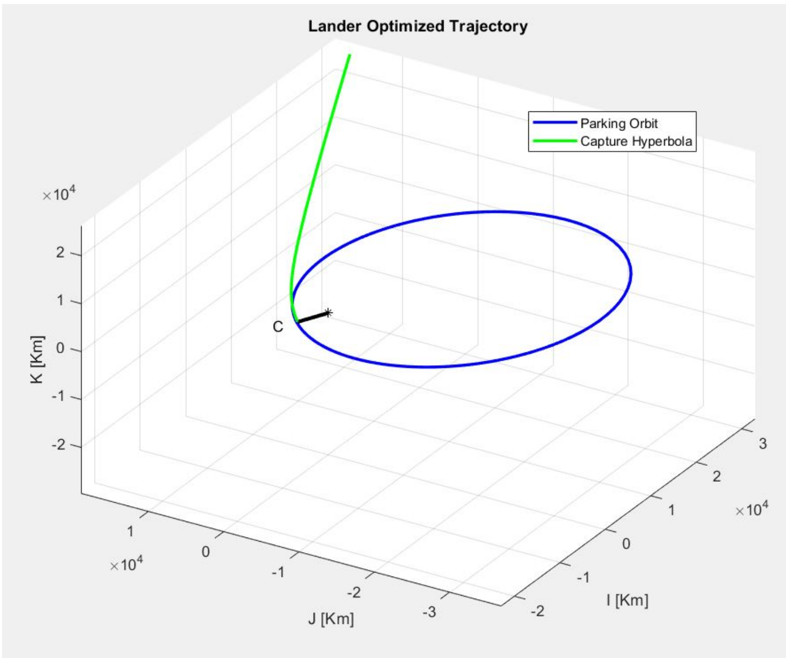

Figure 5.17: 3D Plot for Multi Launch - Different Launch Dates Mission, Lander

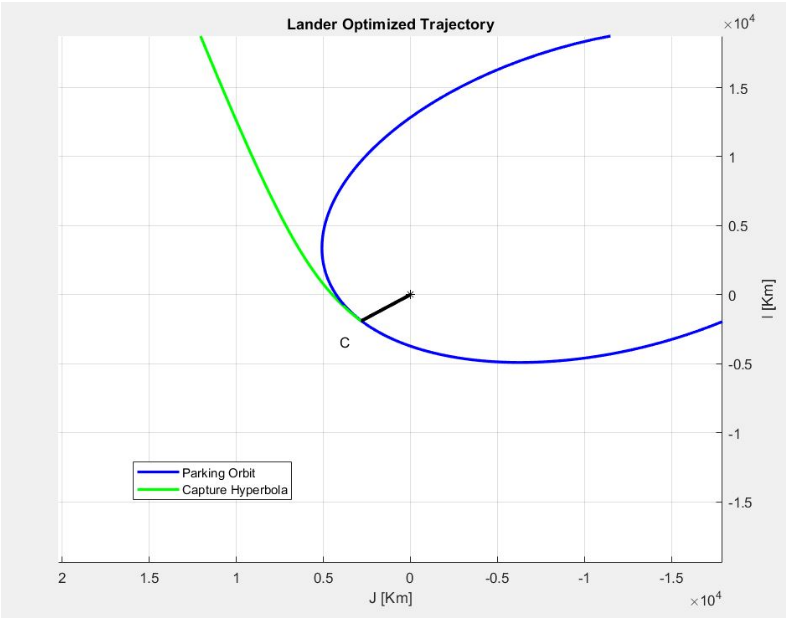

Figure 5.18: Zoom - 3D Plot for Multi Launch - Different Launch Dates Mission, Lander, I-J View

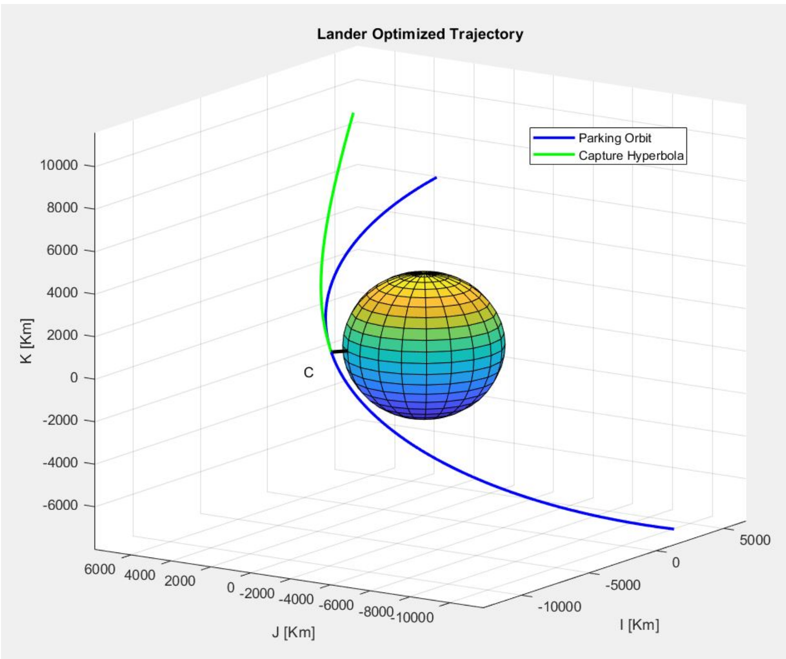

Figure 5.19: Zoom - 3D Plot for Multi Launch - Different Dates Mission, Lander, Capture Maneuver Detail

5.4 Optimization of Eccentricity

Another variable that can be optimized by the *ga* is the eccentricity or the distance of the periapsis. This two quantities are linked by the following relationship:

$$e = 1 - \frac{r_p}{a} \tag{5.2}$$

Thus, leaving the semi-major axis unaltered, a minimum limit of rp is fixed, so that the minimum altitude is 100 Km from the Martian surface. At this point, all that remains is to add two more parameters to be optimized by the genetic algorithm for the mission with two spacecraft:

- $e_{orbiter}$: orbiter parking orbit Eccentricity;
- e_{lander}: lander parking orbit Eccentricity.

For the single launch configuration, instead, only one parameter have been added. In the case of a single launch, therefore, there will be a total of 5 parameters, while in that of the with different mission dates there will be 9 parameters. It is very important to remember to change the maximum limit (LB) of the algorithm so that it makes eccentricity to vary between 0 and e_{max}.
In both analyzes the results are obtained for the maximum eccentricity value, that is $e = 0.8293$, which corresponds to the minimum pariapsis distance. The algorithm tries to maximize eccentricity because, with fixed semi-major axis value, r_p lowers and insertion into the parking orbit tends to cost less at low radii. If instead of optimizing the initial mass, *ga* had to minimize ΔV_{total}, thus, it would have tried to reduce the escape cost, increasing the capture one.
Up to now the costs of ascent and descent maneuvers had remained the same because they were strictly dependent on the geometry of the orbit; in this case can be seen that the descent maneuver will have a small decrease as well as the ascent will cost even less, as generally happens for low r_p.
The algorithm converges relatively quickly also in this case, even if it can be seen that the number of iterations necessary for the optimization has a small increasing, reaching up to about 200 in the case of the two launches.
The considerations made previously regarding a comparison between the two missions are also valid in this case, with the difference that, by optimizing the eccentricity, the mass saving obtained with the multiple launch with different dates becomes 265 Kg. One consideration can be made about the Delta-V: until now costs of the multi launch has been always greater than the single launch because in the first case there are two capture costs. However, with the optimizing of the eccentricity seen in this Section, there is a decrease of the Total ΔV, that becomes similar to that of the single launch configuration.

Maneuver	m_i [Kg]	m_u [Kg]	m_p [Kg]	m_s [Kg]	ΔV [Km/s]
Earth-Mars	3561,09	2758,1	730	73	1,0127
Descent	2380,4	1468,1	829,362	82,936	1,2606
Ascent	568,1236	50	471,0214	47,102	5,19
Mars-Earth	377,66	200	161,51	16,151	2,4634
Total Propellant Mass =2191,89 Kg			$\Delta V_{capt+esc}$=3,476 Km/s		
Optimized Total Mass =3561,09 Kg			ΔV_{tot}=9,936 Km/s		

Table 5.8: Output data: Single Launch Configuration with Optimized Eccentricity

Maneuver	m_i [Kg]	m_u [Kg]	m_p [Kg]	m_s [Kg]	ΔV [Km/s]
			Lander		
Earth-Mars	2989,8	2380,4	554	55,398	0,9046
Descent	2380,4	1468,1	829,3625	82,936	1,2606
Ascent	568,1236	50	471,0214	47,102	5,19
			Orbiter		
Earth-Mars	305,855	203,9558	95,765	9,576	1,658
Mars-Earth	250,513	200	45,92	4,592	0,894
Total Propellant Mass =1996,055 Kg			$\Delta V_{capt+esc}$=3,457 Km/s		
Optimized Total Mass =3295,56 Kg			ΔV_{tot}=9,916 Km/s		

Table 5.9: Output data: Multiple Launch, Different Dates Mission with Optimized Eccentricity

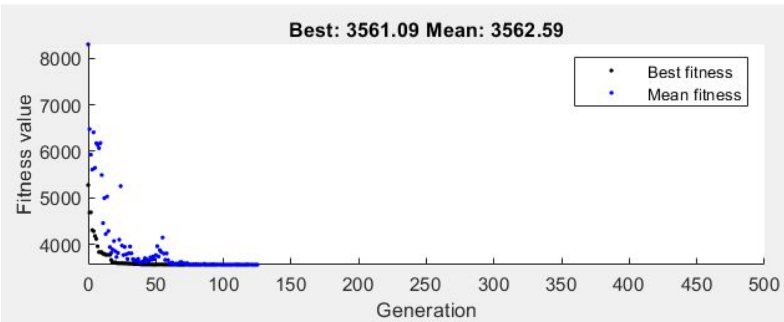

Figure 5.20: Fitness Value - Generation Plot for Single Launch - Optimized Eccentricity

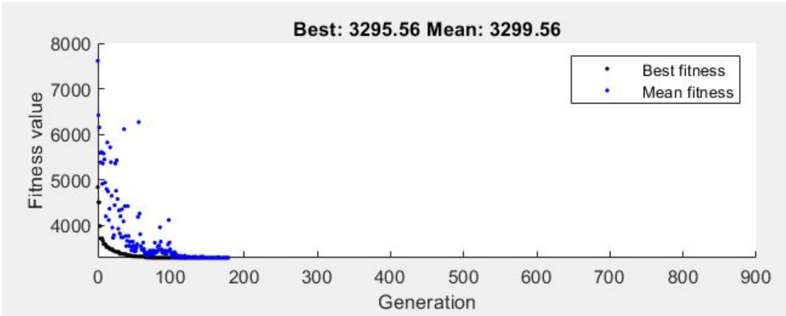

Figure 5.21: Fitness Value - Generation Plot for Multiple Launch, Different Dates - Optimized Eccentricity

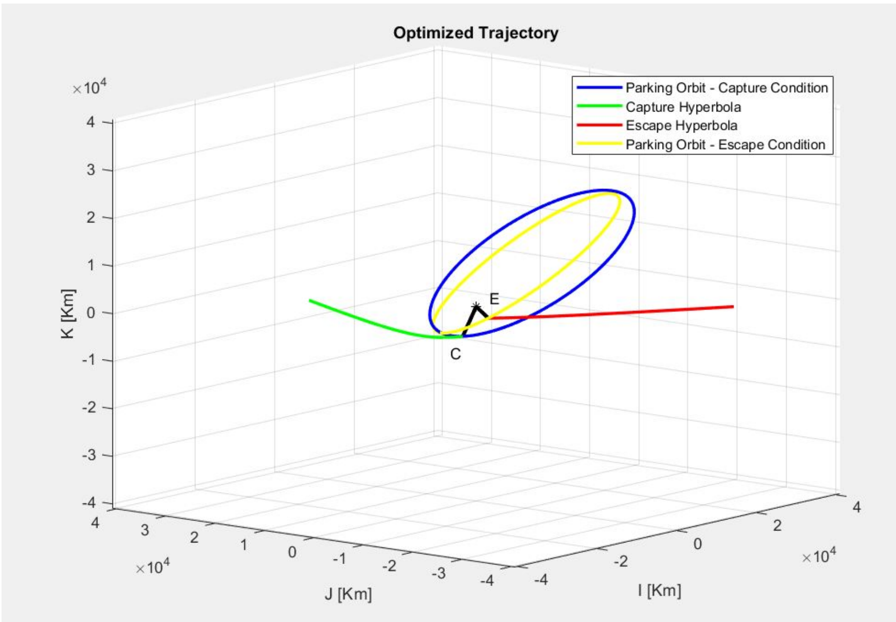

Figure 5.22: 3D Plot for Single Launch - Optimized Eccentricity

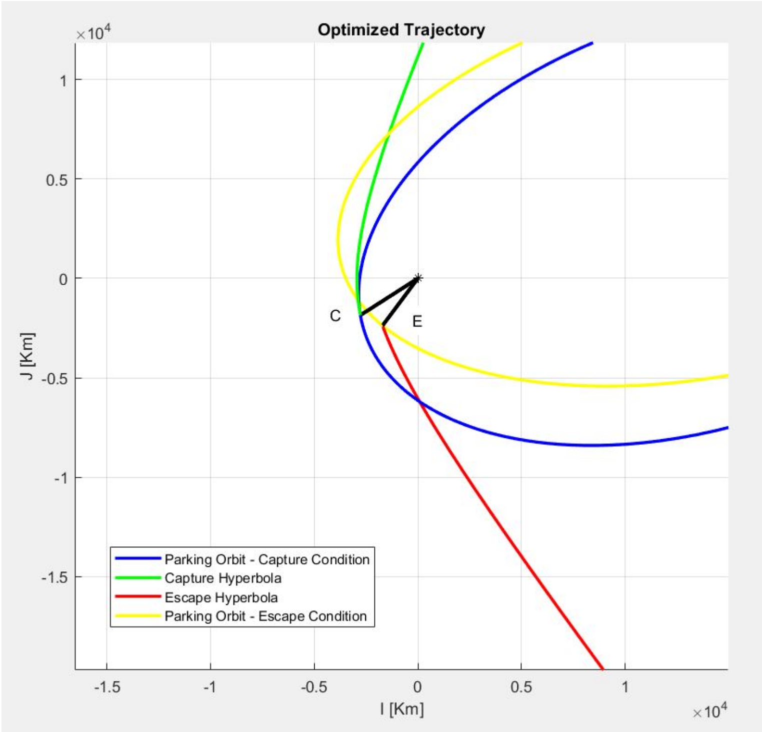

Figure 5.23: Zoom - 3D Plot for Single Launch - Optimized Eccentricity, I-J View

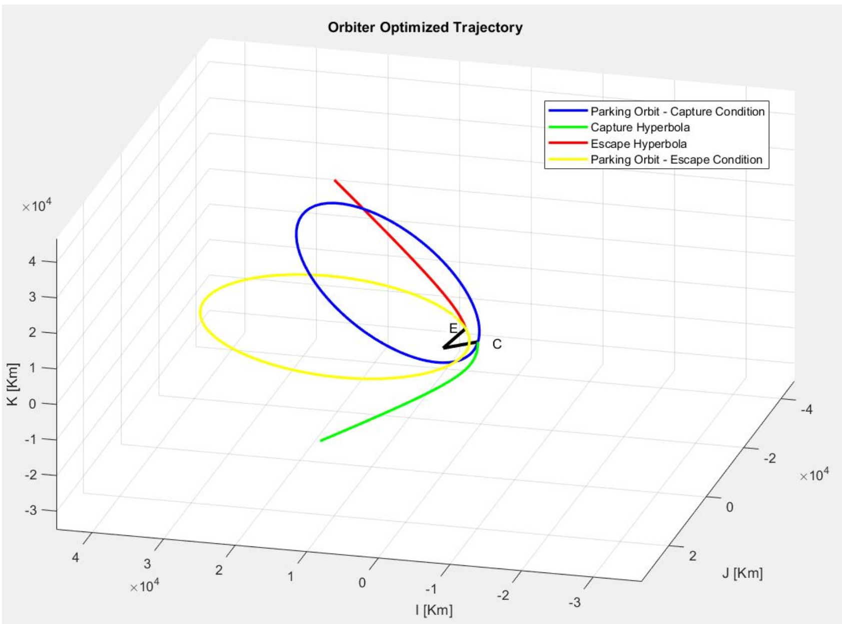

Figure 5.24: 3D Plot for Multi Launch, Different Dates Mission, Orbiter - Optimized Eccentricity

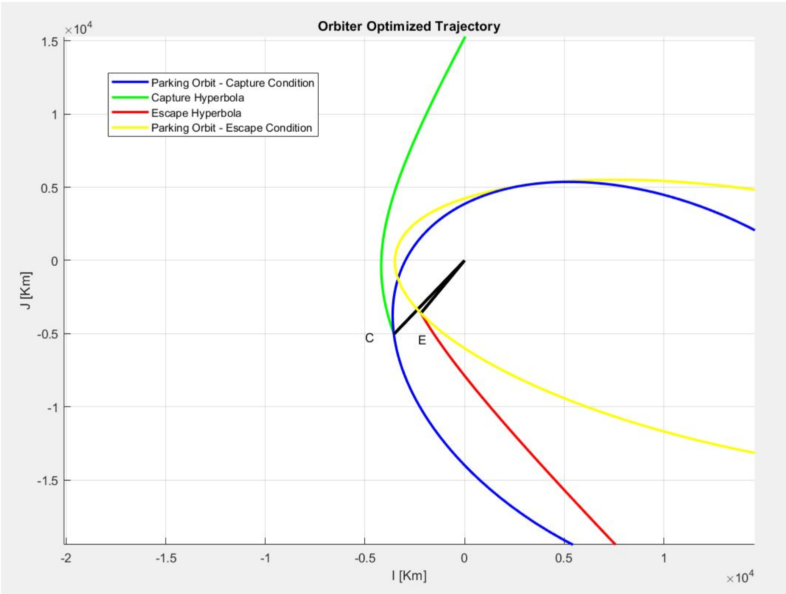

Figure 5.25: Zoom - 3D Plot for Multi Launch, Different Dates Mission, Orbiter - Optimized Eccentricity, I-J View

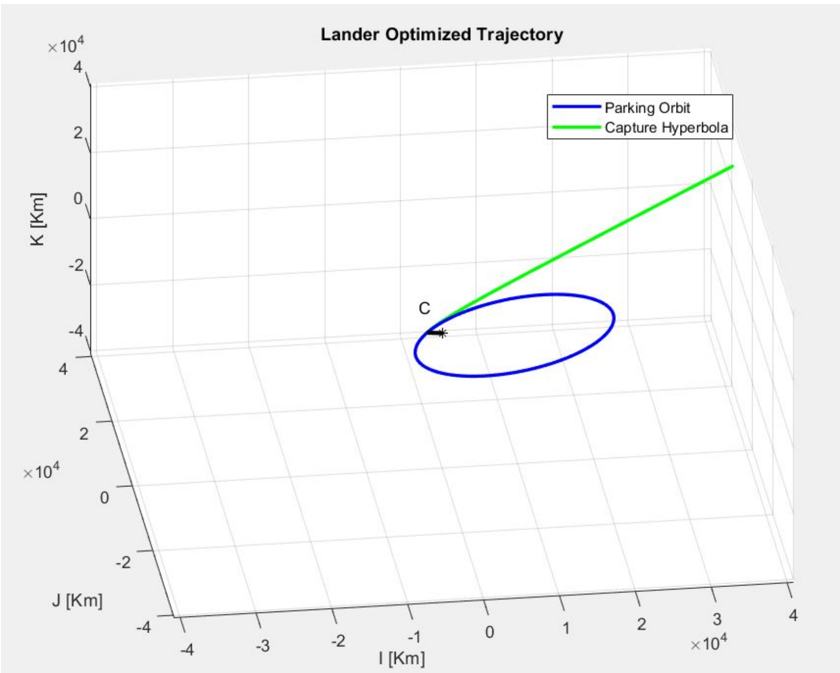

Figure 5.26: 3D Plot for Multi Launch, Different Dates Mission, Lander - Optimized Eccentricity

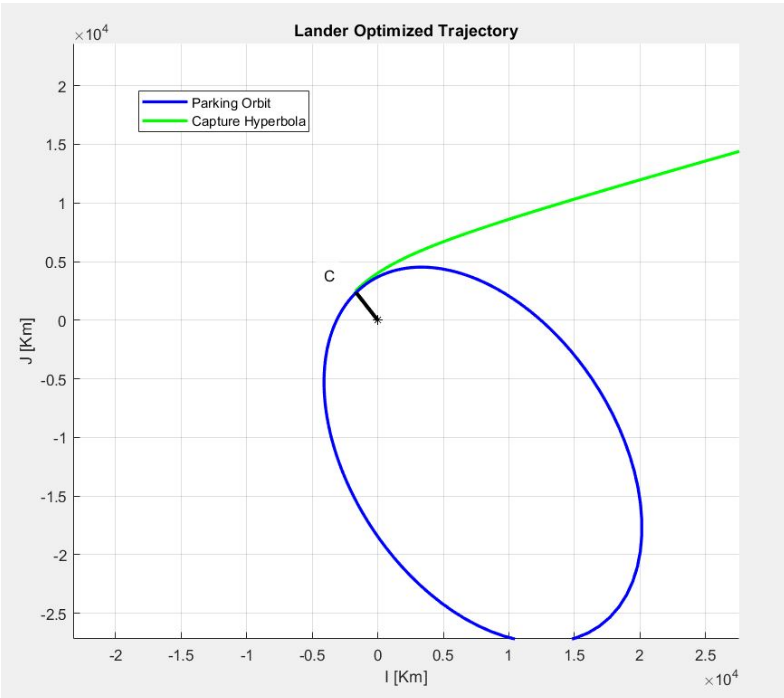

Figure 5.27: Zoom - 3D Plot for Multi Launch, Different Dates Mission, Lander - Optimized Eccentricity, I-J View

5.5 Semi-Major Axis Variation

It might be interesting to study the effects of semi-major axis variation on total mass and ΔV.
Semi-major axis is connected to the eccentricity and radius of the periapsis via the equation:

$$a = \frac{r_p}{1-e} \tag{5.3}$$

For the study has been decided to fix the periapsis distance equal to the input data $r_p = 4089{,}6Km$. Calculation have been made with 3 different values of a:

- 1 sol parking orbit ($\tau = 88775sec$) $\Rightarrow a = 20448Km$;
- 0.75 sol parking orbit ($\tau = 66581{,}25sec$) $\Rightarrow a = 16880Km$;
- 0.5 sol parking orbit ($\tau = 44387{,}5sec$) $\Rightarrow a = 12881Km$.

ΔV_{total} is the sum of all maneuvers (capture, descent, ascent and capture) and the results in Table 5.10 show that this value increases with the rising of semi-major axis. Looking at the individual contributions, it can be seen that the algorithm, by optimizing the initial mass m_{total}, tends to decrease the cost of capture and increase the escape one, since the the capture maneuver is the one that limits more the initial mass.
Regarding the ascent phase, the spacecraft is launched from the surface of Mars. The target is the stopover orbit, whose energy is

$$\epsilon = -\frac{\mu}{2a} \tag{5.4}$$

As the semi-major axis increases, the energy of the parking orbit tends to become bigger, and the spacecraft needs a higher ΔV to reach the orbit. Same considerations can be made for the descent maneuver, where however, the starting point is on the parking orbit and there will be a braking to descend on the Martian surface.

τ [sol]	a [deg]	ΔV_c [Km/s]	ΔV_e [Km/s]	ΔV_{ascent} [Km/s]	$\Delta V_{descent}$ [Km/s]	ΔV_{total} [Km/s]	m_{prop} [Kg]	m_{total} [Kg]
0,5	12881	1,2347	1,6217	5,2058	1,1167	9,1789	2134,8	3493,4
0,75	16880	1,1503	2,398	5,2986	1,2095	10,0564	2362,2	3708,8
1	20448	1,0872	2,4852	5,3498	1,2608	10,183	2388,664	3777,5

Table 5.10: Output data: semi-major axis variation

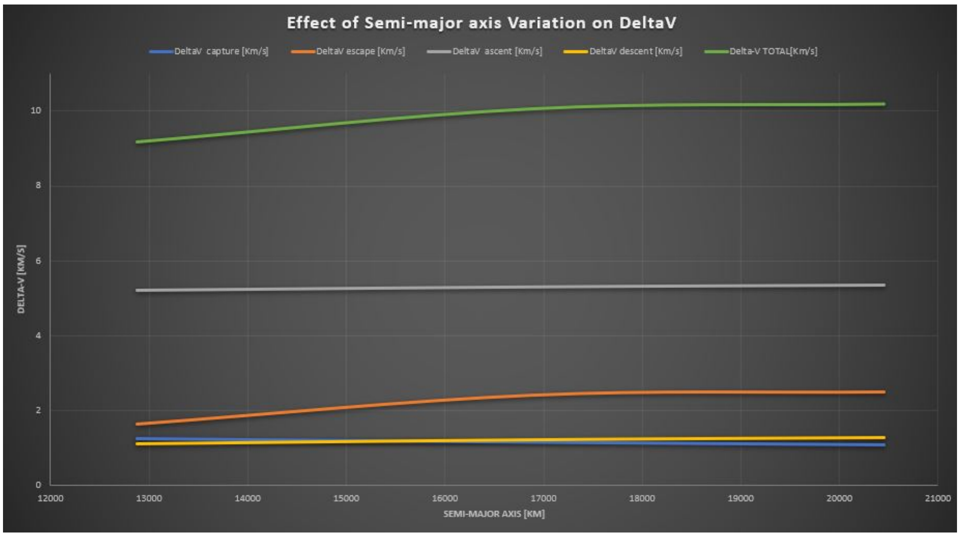

Figure 5.28: Output data graphic: ΔV - Semi-major axis

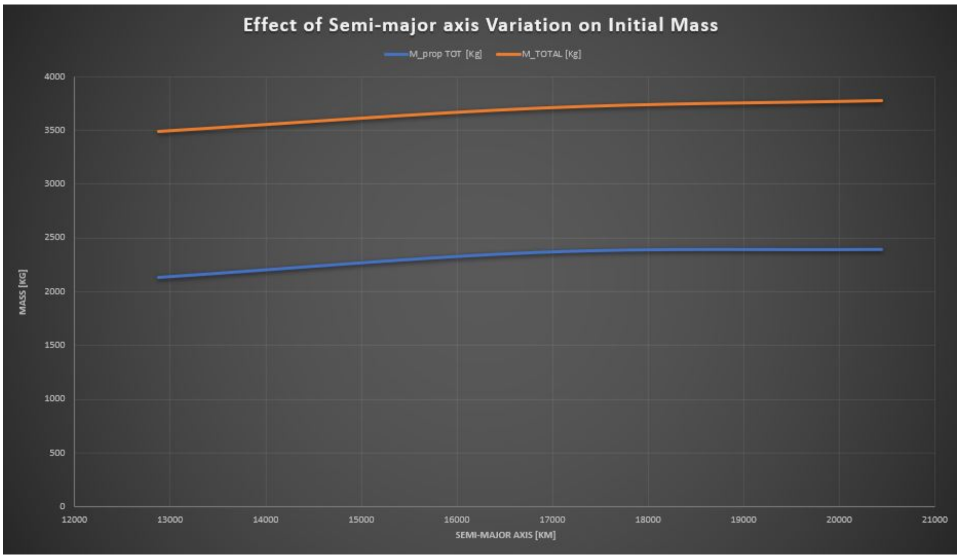

Figure 5.29: Output data graphic: m_{total} - Semi-major axis

5.6 Return Payload Mass Variation

A final case study is worth of interest: the possibility of varying the mass of the payload upon return to Earth. This study has been performed for both the single launch (Section.5.2) and separate launch with different dates (Section.5.3.3) missions and the m_{return} is established to change between $[100 : 1000]$ Kg. Results are shown respectively in Tables 5.11 and 5.12.
In the single launch configuration, as expected, the genetic algorithm tends to increase the cost of capture and decrease the cost of escape. In particular, ΔV_e is reduced faster for lower mass values. The result is a decrease in the total ΔV as the payload raises. As regards the separate launch mission, the total cost of capture and escape remains unchanged. This happens because the algorithm optimizes two different parking orbits. As proof of this, in Figure 5.33 can be observed a fairly linear growth as regards the mass of the orbiter, while that of the lander is left unchanged.

m_{return} $[Kg]$	ΔV_c $[Km/s]$	ΔV_e $[Km/s]$	ΔV_{total} $[Km/s]$	m_{total} $[Kg]$
100	1,0871	2,4897	3,568	3525,8
200	1,0872	2,4852	3,5724	3777,5
300	1,0873	2,4846	3,5719	4027,5
400	1,0874	2,4841	3,5715	4277,4
500	1,0875	2,4835	3,571	4527,3
600	1,0877	2,4831	3,5708	4777,1
700	1,0878	2,4826	3,5704	5027
800	1,088	2,4823	3,5703	5276,8
900	1,0881	2,4819	3,57	5526,6
1000	1,0882	2,4816	3,5698	5776,4

Table 5.11: Output data - Return payload mass variation for single launch

m_{return} $[Kg]$	ΔV_{total} $[Km/s]$	m_{total} $[Kg]$	$m_{orbiter}$ $[Kg]$	m_{lander} $[Kg]$
100	4,074	3314,81	132	3182,8
200	4,074	3533,2	350,45	3182,8
300	4,074	3752,62	569,82	3182,8
400	4,074	3972	789,19	3182,8
500	4,074	4192	1009,2	3182,8
600	4,074	4410,7	1227,9	3182,8
700	4,074	4640,7	1457,9	3182,8
800	4,074	4861,7	1678,9	3182,8
900	4,074	5068,9	1886,1	3182,8
1000	4,074	5288,1	2105,3	3182,8

Table 5.12: Output data - Return payload mass variation for separate launch

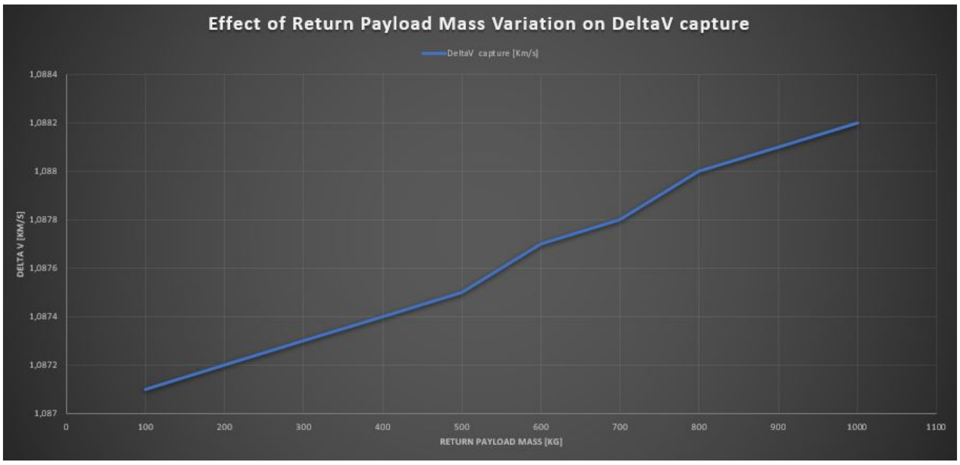

Figure 5.30: Output data graphic for single launch: ΔV_c - return payload mass

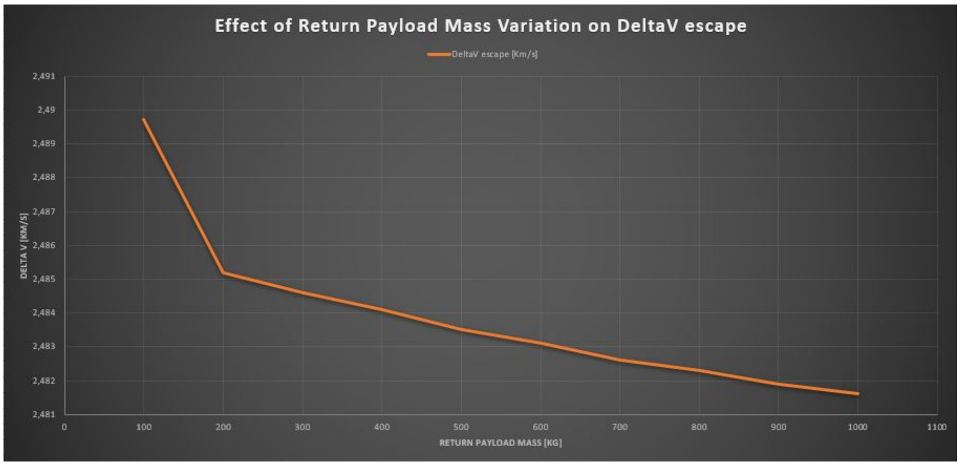

Figure 5.31: Output data graphic for single launch: ΔV_e - return payload mass

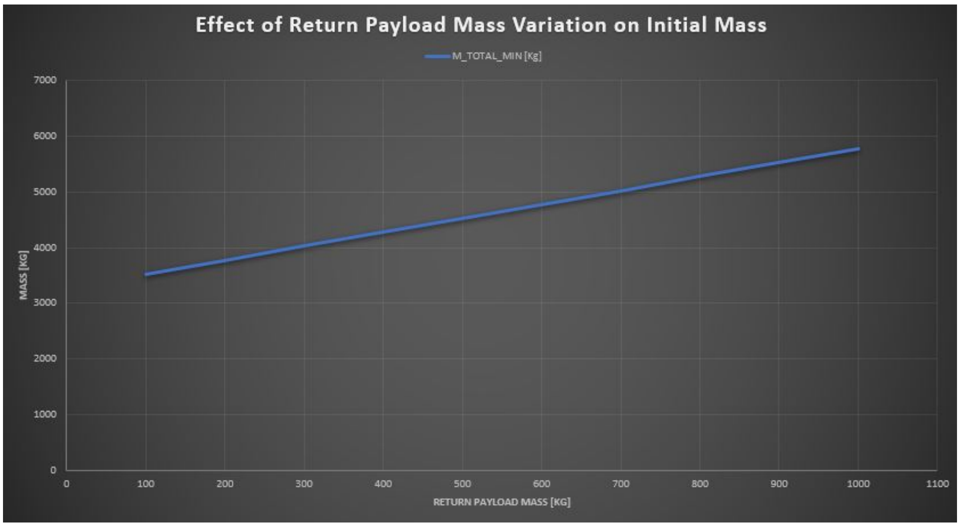

Figure 5.32: Output data graphic for single launch: m_{total} - return payload mass

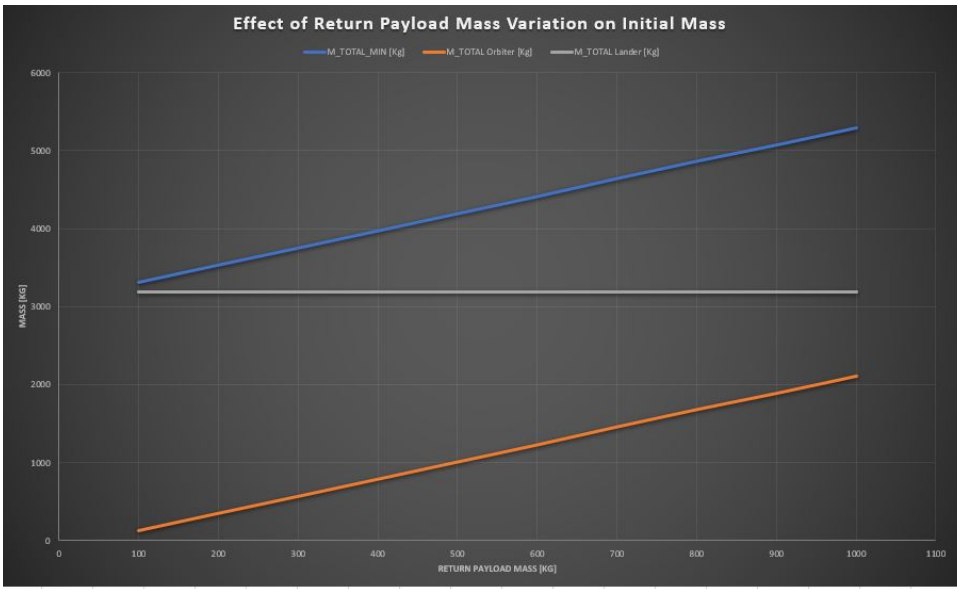

Figure 5.33: Output data graphic for separate launch: m_{total} - return payload mass

Chapter 6

Conclusions

The purpose of this Master Thesis was the development of a computational code able to calculate, using the genetic algorithm, the best orientation of a parking orbit for a round trip mission to Mars and to evaluate the possible advantages of a multi-launch mission. The optimization of the parking orbit and of the capture and escape maneuvers were evaluated through a minimization of the initial mass. The algorithm generated for this thesis may also be effective for studies on other planets or to study the influence of perturbations on a certain mission. Thus, it is a valid tool for carrying out preliminary mission analyzes.
At the beginning of the document, was presented the Sample Return mission led by NASA and ESA, with the aim of highlighting the various phases of the mission, the objectives and its importance for the scientific community. The second part was focused on the genetic algorithm. Its operation and characteristics have been described, explaining why it is widely used for optimization problems such as the one treated in this thesis. The laws of orbital mechanics were explained, and, subsequently, was described in detail the analytical method that has been implemented in the MATLAB code. This algorithm was then applied to four different scenarios, in which the mission has been performed with a single or double launch.
The single-launch mission is the first to be analyzed and achieved the worst results in terms of initial mass. For the double launch configuration with same stopover orbit, mission has been performed by two spacraft, one that has to land on Mars for the collection of samples (lander) and the other that has perform the escape from Mars to bring the samples back to Earth (orbiter). Compared to the previous case, was seen a mass saving of about 70 kg. Complicating the problem, was then studied the double launch case with two parking orbits with different orientation, which reported a decrease in the initial mass of about 150 kg compared to the single launch case. Finally, different launch times were entered for the orbiter and lander to analyze how the total costs would change. The lander leaves first, with an arrival on Mars scheduled for 2040, and then, in 2042, the orbiter will arrive and take the samples bringing them back to our planet. The result obtained by this

configuration are the best of all the case studies with a saving in mass of 240 Kg compared with the single launch mission.
Thus the advantages of the multi launch configurations have been verified.
By optimizing the eccentricity value to the genetic algorithm, it has been seen that the performances in terms of mass and mission cost improve and the advantage of the two-launch mission becomes greater.
The study focused on the semi-major axis have shown that lower a value has a positive impact on the total cost of the mission, at fixed periapsis value, as it lowers the cost of the descent and ascent maneuvers, even if there are some disadvantages due to the increase in the cost of capture. Finally, the influence of the return payload variation was evaluated. It was concluded that the multi-launch mission becomes more advantageous for high return payloads and the total cost of the mission remains costant.
Future implementations could allow more precise analyzes, for example studying how to target a particular landing site, or how to best provide for communications coverage. Furthermore, the ascent phase could be studied more carefully, exploring the possibility of using the hybrid propulsion or a multi-stage configuration of the MAV.

Appendix A

MATLAB code Validation

Referring to Chapter 5 , here are shown the results related to the validation of the MATLAB code used for the analyzes. The data used for the validation have been taken from the paper *'Optimum Parking Orbit Orientation for a Three-Dimensional Capture-Escape Mission'* [22] and are listed in the table A.1. To establish if the

Input Parameters		
Stopover Orbit		
Semi-major axis a	19.550	Km
eccentricity	0.8	
inclination	170	deg
Capture Hyperbola		
$C3_c$	20.6	Km^2/sec^2
right ascension α_c	138	deg
declination δ_c	5.9	deg
Escape Hyperbola		
$C3_e$	57.6	Km^2/sec^2
right ascension α_e	31.6	deg
declination δ_c	8.9	deg

Table A.1: Paper Input Data Parameters

code generated for the thesis is valid, the requirement is that the optimization by genetic algorithm minimizes the Delta-V, and this value has to be very close to the paper one. MATLAB *ga* settings is:

```
[optimal parameters, DELTA_V_MIN, val,output,population,scores]=
ga(@mission1_optim_dv,4,[],[],[],[],LB,UB,[],options)
```

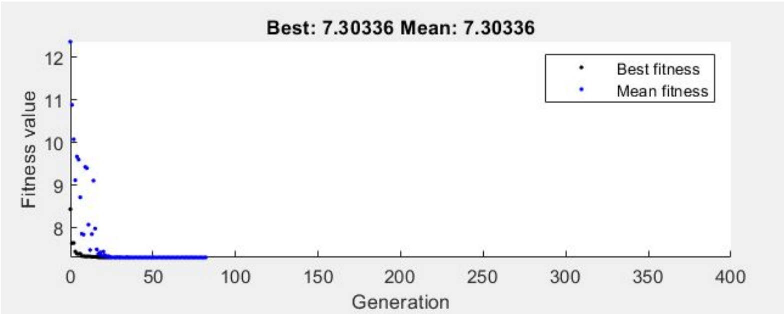

Figure A.1: Fitness Value - Generation plot for paper data

The results of this analysis are relative to the 'Unperturbed Mars Mission' data from the paper (Table1-b of the paper).
In Table A.2 is shown the comparison between the results of the paper and the MATLAB code. As can be seen from the data, the ΔV is almost the same, thus the code validity is demonstrated. A comment regarding the values of the other four parameters: their values are precisely those that are varied by the algorithm to obtain the optimization. Then *ga* starts from random values and at the end of the convergence, it is clear that these parameters tend towards the target ones.

Paper Optimum Conditions			
Delta-V	ΔV	7.309	Km/sec
Argument of periapsis	ω	349.75	deg
Right Ascension of the ascending node	Ω	156.12	deg
Capture position angle	ρ_c	277.29	deg
Escape position angle	ρ_e	45.4	deg
MATLAB Optimum Conditions			
Delta-V	ΔV	7.30336	Km/sec
Argument of periapsis	ω	357.89	deg
Right Ascension of the ascending node	Ω	166.412	deg
Capture position angle	ρ_c	286.53	deg
Escape position angle	ρ_e	52.99	deg

Table A.2: Output Data - Paper Comparison

Bibliography

[1] National Research Council, *'Assessment of Mars Science and Mission Priorities'*, Washington, DC: The National Academies Press, 2003 (Chapter 11 & 12), doi: 10.17226/10715.

[2] Mars Exploration Program Site, NASA,https://mars.nasa.gov/

[3] MEPAG (2020), *'Mars Scientific Goals, Objectives, Investigations, and Priorities: 2020'* D. Banfield, ed., 89 p. white paper posted March, 2020 by the Mars Exploration Program Analysis Group (MEPAG) at https://mepag.jpl.nasa.gov/reports.cfm.

[4] Brian K. Muirhead, *'Mars Sample Return Campaign Concept Architecture'*, A White Paper for the Planetary Science and Astrobiology Decadal Survey 2023-2032, Jet Propulsion Laboratory, California Institute of Technology.

[5] Mars Sample Return, European Space Agency, https://www.esa.int/Science_Exploration/Human_and_Robotic_Exploration/Exploration/Mars_sample_return

[6] E. Joffre, U. Derz, M. Perkinson, J. Huesing, F. Beyer, J.S. Perez *'Mars Sample Return: Mission Analysis For an ESA Earth Return Orbiter'*, 2nd International Mars Sample Return 2018.

[7] National Aeronautic and Space Administration (NASA) *" Mars 2020 Perseverance Launch Press Kit"* , june 2020.

[8] Mars 2020 rover mission of NASA/JPL, eoportal, https://directory.eoportal.org/web/eoportal/satellite-missions/m/mars-2020

[9] B. K. Muirhead, C. D. Edwards, Jr., A. E. Eremenko, A. K. Nicholas, A. H. Farrington, A. L. Jackman, S. Vijendran, L. Duvet, F. Beyer, S. Aziz *'Sample Retrieval Lander Concept For a Potential Mars Sample Return Campaign'*, Ninth International Conference on Mars, 2019.

[10] Ashley A.Chandler, BrianJ.Cantwell, G.ScottHubbard, ArifKarabeyoglu, *'Feasibility of a Single Port Hybrid Propulsion System for a Mars Ascent Vehicle'*, Elsevier, Acta Astronautica Volume 69, Issues 11–12, December 2011, presented during the 61st IAC in Prague.

[11] A.J.Brown, C.E.Viviano, and T.A.Goudge, *'Olivine-Carbonate Mineralogy of Jezero Crater'*, Research Article, 21 February 2020, https://doi.org/10.1029/2019JE006011

[12] Sourabh Katoch, Sumit Singh Chauhan, Vijay Kumar. *'A review on genetic algorithm: past, present, and future'*, Springer Science+Business Media, LLC, part of Springer Nature 2020, published online: 31 October 2020.

[13] Andrew N. Sloss, Steven Gustafson. *2019 'Evolutionary Algorithms Review'*, arXiv:1906.08870v1 [cs.NE], 3 Jun 2019.

[14] Dan Simon. *'Evolutionary Optimization Algorithms'*, John Wiley & Sons, 2013.

[15] https://www.tutorialspoint.com/genetic_algorithms/

[16] Mathworks, *'Genetic Algorithm and Global Optimization Toolbox Documentation'*, 2020. https://it.mathworks.com/help/gads/index.html?s_tid=CRUX_lftnav

[17] Roger.R.Bate, Donald.D.Mueller, Jerry.E.White *'Fundamentals of Astrodynamics'*, Dover Publications Inc., New York, 1971.

[18] Craig A. Kluever, *'Encyclopedia of Physical Science and Technology'*, Third Edition, Academic Press, 2003.

[19] D. A. Vallado, *'Fundamentals of Astrodynamics and Applications'*, Hawthorne, California, Microcosm Press, 2013.

[20] Seefelder, Wolfgang, *'Lunar Transfer Orbits Utilizing Solar Perturbations and Ballistic Capture'*, Munich: Herbert Utz Verlag. p.76. ISBN 3-8316-0155-0. Retrieved July 3, 2018.

[21] Tyler M. Chlapek, *'Design and Optimization of a Mars Sample Rwturn Mission With Nuclear Thermal Rockets'*, University of Missouri, Dec. 2011.

[22] D. E. Cornick, L. K. Seversike, *'Optimum Parking Orbit Orientation for a Three-Dimensional Capture-Escape Mission'*, Iowa State University, Ames, Iowa, Nov. 1970.

[23] Min Qu, Raymond G. Merrill, Patrick Chai and David R. Komar, *'Optimizing Parking Orbits For Roundtrip Mars Missions'*, Conference Paper, Document ID:20170008844, 2017.

[24] Laura M. Burke, Robert D. Falck, and Melissa L. McGuire *'Interplanetary Mission Design Handbook: Earth-to-Mars Mission Opportunities 2026 to 2045'*, Glenn Research Center, Cleveland, Ohio.